Gas Turbine Laboratory
Department of Aeronautics and Astronautics
Massachusetts Institute of Technology
Cambridge, MA 02139

FINAL TECHNICAL REPORT
on Grant NAG3-1567

entitled

INLET DISTORTION IN ENGINES ON VSTOL AIRCRAFT

submitted to

NASA Lewis Research Center
21000 Brookpark Road
Cleveland, OH 44135

Dr. Colin Drummond
Technical Monitor

PRINCIPAL
INVESTIGATOR: Dr. Choon S. Tan
Principal Research Engineer
Gas Turbine Laboratory

CO-INVESTIGATOR: Edward M. Greitzer
H.N. Slater Professor of Aeronautics and Astronauti
Director, Gas Turbine Laboratory

May 1994

INLET DISTORTION IN ENGINES ON VSTOL AIRCRAFT

Executive Summary

This report presents the results of a research program on "Inlet Distortion in Engines on VSTOL Aircraft" carried out at the MIT Gas Turbine Laboratory during the period October 1989 - December 1993. The program focused on: (1) the development of three-dimensional flow computational methodology for predicting the effects of nonuniform flow on the performance of aircraft engines in VSTOL aircraft; (2) the development of a three-dimensional instability analysis of flow in multi-stage axial compressors; and (3) the *preliminary* applications of these newly-developed methodologies for elucidating the effects of flow three-dimensionality. The accomplishments of the program are brought out when the current status of predictive capabilities for three-dimensional flow instabilities in compressors is assessed against that in 1989.

1.0 Introduction

This document constitutes a final report for a research program on "Inlet Distortion in Engines on VSTOL Aircraft" sponsored by NASA Lewis Research Center under Grant NAG3-953 with Dr. Colin Drummond as Technical Monitor. The report is organized as follows. The background that motivated the initiation of this research program will first be presented. The technical objectives of the program and the approach adopted are then delineated. Next, we describe the predictive methodologies that have been developed to address the response of aircraft engines to inlet flow nonuniformities (with radial and circumferential variation) and the stability of multi-stage compressors for which flow three-dimensionality is important. Assessment of the methodologies against known analytical results will be made. We also present results from our preliminary examination of the effects of flow three-dimensionality on the response of aircraft engines to inlet distortion and on the stability of multi-stage compressors. Finally, we summarize the accomplishments of the research program, and describe where we stand in terms of: (i) multi-stage compressor 3-D stability predictive capability, (ii) methodology for computing the response of the engine to inlet distortion, and (iii) methods for computing the nonlinear evolution of engine instability.

2.0 Technical Background

The reingestion of hot exhaust gases (that originate from the nozzles) into a VSTOL aircraft's aeroengine intake can give rise to a non-uniform stagnation temperature and stagnation pressure distribution at the inlet face of the compressor [1]. Moreover, for near-ground maneuvers, the resulting flowfield configuration in the immediate neighborhood of the VSTOL aircraft can be such that there exists a high potential for the development of strong streamwise vorticity; this could assume the form of an inlet vortex stretching from the ground or the fuselage into the engine intake. Such situations of non-uniform inlet flow can cause a major loss in performance and affect the aerodynamic stability boundary of the compression system in an adverse manner. As a consequence, the engine may encounter rotating stall and surge, aerodynamic instabilities which are detrimental to the engine and aircraft performance.

Because of the importance of quantifying stability and performance, it is necessary during the course of developing a VSTOL aircraft that extensive model and prototype tests be implemented to measure the extent of hot gas reingestion over a wide range of aircraft maneuvers. Based on these test data, empirical correlations are then devised for estimating the associated loss of engine performance. These correlative approaches employ a limited test database, so the resulting uncertainty associated with its application to advanced aeroengine designs can be considerable. Furthermore, such a correlative approach does not reflect the basic fluid dynamics underlying the resulting loss in performance and stability margin. A predictive methodology for addressing the effects of hot gas reingestion and other general forms of inlet distortion (for which flow three-dimensionality is significant) would thus be a useful tool in the development of aeroengines for VSTOL applications. Such a methodology was nonexistent at the initiation of this research program. *One objective of the research effort was thus the development of a computational methodology for predicting the effects of non-uniform flow on the performance of aircraft engines on VSTOL aircraft.*

The aerodynamic interaction between different engine components can have a major effect on the behavior of the individual flowfields, and it is critical that any computational methodology

developed have the capability to include the effects due to such interactions. For instance, the effect of interaction between the compressor and intake [1] on the inlet flowfield can be discerned from the results of Fig. 1, in which the presence of an aeroengine (compressor) affects the upstream flow in the inlet operating at incidence. At 30° incidence without the aeroengine (Fig. 1a), the flow separated off the lip of the inlet with the formation of a large region of low stagnation pressure fluid. However, with the aeroengine, even when operating at a larger incidence of 35°, the extent of separation flow is much smaller (Fig. 1b vs. Fig. 1a). The reduction in the size of separated flow is a result of the fact that a lower inlet flow velocity in the separated flow region corresponds to the compressor operating with a larger pressure rise and hence a more favorable pressure gradient. The interaction between engine components can thus have an important bearing on stability assessment and the interpretation of data from distortion tests on isolated compressors, and it is important that the resulting methodology includes such effects (e.g. spool-spool interactions in multi-spool compressors) in a consistent manner when assessing engine response to inlet distortion. It should also be noted that the methodology to be developed can be used to address compressor stability problems for which the flow non-uniformities are self-induced (i.e. internal flow distortion rather than inlet flow distortion which is externally imposed).

For the flow situations encountered in VSTOL aircraft, the three-dimensionality in the (engine) compressor response is due to externally imposed distortion. However, recent experimental data of Day [2] and MIT/GE [3] also point to the importance of three-dimensionality in compressor instability phenomena, *even in situations that were thought to be nominally two-dimensional.* In particular, the data [2], [3] indicate that there are two routes to stall even in high hub-to-tip ratio multistage compressors: (i) a long wavelength or "modal" type of stall precursor which is essentially two-dimensional [2] - [5]; and (ii) a short wavelength type with an inherently three-dimensional structure [2], [3]. The first of these constitutes a flow disturbance with a wavelength of the order of the circumferential length of the compressor annulus and is observed to span the region from hub to tip. The waves associated with these precursors propagate about the annulus at a phase speed usually between 0.2 to 0.4 times the rotor speed. The sequence of events

is that small amplitude long wavelength disturbances grow in intensity, finally evolving into a fully developed stall cell as the compressor is throttled toward the stall point.

In contrast, the short wavelength type of stall precursor is not two-dimensional and is characterized by strong three-dimensionality. As the operating point of the compressor approaches stall, this type of precursor disturbance has been observed to appear near the blade tip (usually in the first rotor for multistage compressors representative of current design) and to cover a circumferential extent of a few blade pitches only. During the stall inception process, the short wavelength type of disturbance is observed to propagate circumferentially at a speed approximately three-quarters of the rotor speed. As the compressor stalls, the disturbance grows radially as well as circumferentially in extent, and its propagating speed decreases to a value approximately 0.4 to 0.5 times rotor speed.

The two-dimensional flow model that has been developed [6] - [10] has been successful in addressing the stability issues in compressors which exhibit long wavelength stall disturbances, but there are clearly important practical situations in which this model does not apply. To describe these situations, a three-dimensional flow model needs to be developed. This is especially relevant to machines of low hub-to-tip ratio as well as fans. *Thus, during the course of the research program, it was deemed necessary to initiate a complementary task on the development of a 3-D instability analysis of flow in multi-stage axial compressors.*

In summary, while the research program was initiated to address the response of aircraft engines to inlet distortion where three-dimensional effects must be considered, a parallel and complementary effort was also initiated to examine the importance of three-dimensionality in compressor instability. It is anticipated that analytical/computational procedures developed in the program will provide useful tools in the development of effective management techniques for these aerodynamic instabilities in modern axial compressors. In the next section, the technical objectives are delineated in the light of the above technical background.

3.0 Technical Objectives

The overall goal of the research program was to develop the capability to predict: (i) the response of multi-stage compressors to externally imposed and self-induced flow distortion of the three-dimensional type; and (ii) the manner in which multi-stage compressors stall. This necessarily involved the formulation of a physical flow model for a multistage compressor and the compression system representing the aircraft engine. It also included the development of rational computational models for assessing the stability of three-dimensional flow through a multistage compressor/fan and for examining the development of these nonlinear instabilities. More specifically, to achieve the overall goal the following technical tasks have to be implemented:

1) ***Physical representation of blade-row and compressor:***

   Development of a physical flow model for computing the performance and response of a multistage compressor (and each blade row making up the multistage compressor) to unsteady and non-uniform flow. The unsteadiness and non-uniformities could be compressor self-induced or externally imposed.

2) ***Integration of upstream flowfield, flowfield in between blade-rows, and downstream flowfield with compressor:***

   Consistent integration of an upstream flow model and a downstream flow model with the compressor model from (1) must be carried out. In mathematical terms, the compressor serves as the boundary condition that generates the disturbance flow upstream and downstream of the compressor. This is also true for the blade rows in relation to the space between the blade rows.

3) ***Computational procedures for stability prediction:***

   Development of computational procedures for assessing the stability of a compressor and a compression system representing an aircraft engine when subjected to a general three-dimensional unsteady flow disturbance.

4) ***Computational procedure for development of compressor instabilities:***

   Development of a computational procedure to compute the temporal and spatial nonlinear

evolution of initial compressor instability into rotating stall.

5) ***Inlet conditions for initiation of instability:***

Use of the methodologies developed in (3) and (4) for establishing the inlet flow conditions under which compressor instability can occur.

6) ***Causal relation between inception of instabilities and design characteristics of compressor:***

The research not only addresses the use of methodologies developed in (3) and (4) to examine compressor stability issues but also the establishment of causal links between the inception of instabilities and the design characteristics of the compressor. As an example, because of the implications for dynamic control, one would like to be able to predict the route to compressor instability (short wavelength type of stall precursor *vs* long wavelength) based on the knowledge of compressor design characteristics.

7) ***Definition of necessary experimental investigations:***

Finally, it was anticipated that the results from the research program will be used to critically assess what are the most useful experimental investigations that need to be carried out to further quantify the technical issues addressed here.

4.0 Technical Approach

One might envisage obtaining compressor performance and response to unsteady and non-uniform flow by direct computation of flow through the compressor. Even a rudimentary attempt to assess the computational capabilities needed, however, shows clearly that this is not even close to being feasible given current and near-term foreseen computational technology [11]. It is thus essential to develop models for the compressor dynamic behavior. Such an approach has been shown to be extremely valuable for assessing the stability and response of compressors, in terms of performance as well as stability, when operating with circumferential distortion as long as the overall flow is essentially two-dimensional [6] - [10].

The approach that has been taken involves modelling of the response of the individual blade passage to the non-steady, 3-D, non-uniform flow in terms of the relevant fluid dynamic

features (in a blade passage) and then calculating the response of the overall compression system. Such an approach has been adopted in the development of methodologies for addressing the three-dimensional aspects of stability issues for compressors operating in the uniform as well as distorted flow environment. In essence, the approach adopted here seeks to strike an optimal balance between computational and intellectual resources.

In the following, the development of the methodologies based on the approach alluded to in the above will first be described.

5.0 Development of Predictive Methodologies

This section will be organized as follows. We will first present the overall conceptual approach involving the flow modelling of technical tasks (1) and (2) of Section 3.0. The quantitative aspects of a physical flow model for computing the performance and response of a multi-stage compressor to unsteady and non-uniform flow are described next; this is followed by the computational procedure (i.e. technical task (4)) for implementing the computational flow model from technical tasks (1) and (2). This essentially yields a predictive tool that enables one: (i) to compute the response of a compressor, measured in terms of performance and stability, to flow non-uniformities; and (ii) to compute the temporal and spatial nonlinear evolution of initial instability into rotating stall/surge.

While the above methodology can be quite general, a more effective (and direct) way for examining the nature of compressor instability inception and its link to compressor characteristics is a linear stability calculation for examining the unsteady behavior of a general three-dimensional disturbance flow imposed upon a steady background flow in a multi-stage compressor. This essentially constitutes task (3) of Section 3.0. The development of the theoretical and computational framework for implementing such a three-dimensional calculation for multi-stage compressors will be discussed and presented in Section 6.0. The availability of such a calculation procedure would enable one: (i) to determine the most unstable modal disturbance and its spectral content; (ii) to establish the link between compressor design parameters and flow instability

inception; (iii) to provide the initial condition for the computational procedure to technical task (4) for examining the temporal and spatial nonlinear evolution of initial compressor instability into rotating stall/surge; and last but not least (iv) to provide a plant model for active control of low hub-to-tip ratio compressors/fans. Thus, the two methodologies are complementary to one another, as indicated above.

5.1 Overall Conceptual Approach

The key concepts in the approach for the development of a general methodology for computing the response of aircraft engines to 3-D inlet distortion and for computing the evolution of 3-D flow instabilities are elucidated in Figs. 2 and 3. Both the upstream and downstream flowfields perceive the presence of the compressor/fan as a body force distribution. In the situation where the flow is unsteady, the body force distribution should include the inertia force distribution within the compressor due to flow unsteadiness (see Section 5.3). For the flow situation of interest here, the flowfield external to the compressor/fan can adequately be described by the 3-D unsteady Euler equations. The body force distribution that represents the compressor then appears as an additional source term in the Euler equations.

The approach can now be conceptually described as follows. Suppose the flowfield at the inlet face of the compressor/fan at a particular time is known/given, then:

1) Use the flow model for the compressor (see Section 5.3) to compute the flowfield within the compressor. This computed information is used to calculate/update the body force distribution within the compressor, and hence the source term in the Euler equations (see Section 5.3 for more details);
2) Update the entire flowfield;
3) Proceed to the next time level by repeating steps (1) and (2) until no further changes are observed in the solution or the solution has reached equilibrium state with a (periodic) temporal variation.

As one can deduce from the above, the entire procedure can be implemented in a time

accurate fashion. The conceptual approach is a general one; it can be used to calculate the response of the compressor to flow nonuniformity as well as to compute the flow instability inception process, including the (nonlinear) temporal and spatial evolution of flow instability. If gaps between the blade rows are to be included, then the blade-gap flowfield can be adequately described by the unsteady 3-D Euler equations where each blade row is perceived as a body force distribution. Such an approach would allow for flow interactions among engine components in a consistent manner.

There is no limitation to applying the above conceptual approach for addressing stability issues in high speed compressors. However, during the course of developing the computational methodology, it was best to assess the conceptual approach by applying it to low speed multi-stage compressors where the computed results can be compared against known analytical (as well as experimental) results. In what follows, we will first present the governing equations followed by the development of an adequate computational flow model for the compressor response to unsteady and nonuniform flow. We then describe the numerical technique for the solution of the resulting governing equations.

5.2 Governing Equations

The incompressible unsteady 3-D Euler equations can be written in cylindrical coordinates (r,θ,z) as

$$\frac{\partial \vec{U}}{\partial t} + \frac{\partial \vec{F}}{\partial r} + \frac{\partial \vec{G}}{\partial \theta} + \frac{\partial \vec{H}}{\partial z} = \vec{S} \tag{1}$$

with

$$\vec{U} = \begin{bmatrix} 0 \\ rU \\ rV \\ rW \end{bmatrix}, \quad \vec{F} = \begin{bmatrix} rU \\ r\left(U^2 + P\right) \\ rUV \\ rUW \end{bmatrix}, \quad \vec{G} = \begin{bmatrix} V \\ UV \\ V^2 + P \\ VW \end{bmatrix}, \quad \vec{H} = \begin{bmatrix} rW \\ rUW \\ rVW \\ r\left(W^2 + P\right) \end{bmatrix}, \quad \vec{S} = \begin{bmatrix} 0 \\ V^2 + P \\ -UV \\ 0 \end{bmatrix}$$

where (U,V,W) denotes respectively the radial, circumferential, and axial components of velocity,

and P denotes the static pressure; the velocity components and the pressure have been made dimensionless based on the mean wheel speed and the density. The incompressible flow equation has been cast in conservation form for ease in applying the standard numerical solution technique (see Section 5.4 for details).

Equation (1) can adequately describe the flowfield upstream and downstream of a compressor as well as that within the blade gap. However, within the compressor (or each blade row), the flowfield is assumed to be locally axisymmetric at each circumferential position and that this flowfield is compatible with the upstream and downstream flowfield at all times; the effects of pressure change are appropriately described in terms of a body force distribution. Thus, locally at each circumferential position, the flowfield within the compressor or blade row satisfies

$$\frac{\partial \vec{U}}{\partial t} + \frac{\partial \vec{F}}{\partial r} + \frac{\partial \vec{H}}{\partial z} = \vec{S} \tag{2}$$

with

$$\vec{U} = \begin{bmatrix} 0 \\ rU \\ rV \\ rW \end{bmatrix}, \quad \vec{F} = \begin{bmatrix} rU \\ r\left(U^2 + P\right) \\ rUV \\ rUW \end{bmatrix}, \quad \vec{H} = \begin{bmatrix} rW \\ rUW \\ rVW \\ r\left(W^2 + P\right) \end{bmatrix}, \quad \vec{S} = \begin{bmatrix} 0 \\ V^2 + P + rf_r \\ rf_\theta \\ rf_z \end{bmatrix}$$

where (f_r, f_θ, f_z) $(= \vec{f})$ denote the radial, tangential and axial component of the body force distribution.

Equation (2) can be viewed as a result of suppressing the θ-dependence in the equation of motion and including its effects on the flowfield in the body force $\vec{f}$. In general, the body force within a compressor consists of a portion associated with the steady pressure rise and a portion associated with the inertia of the fluid within the rotor and stator blades. The success of the proposed approach thus depends on our ability to include the relevant features of the fluid dynamic response of a compressor in $\vec{f}$ (or equivalently f_r, rV, f_z). While the above exposition might appear to indicate that the flowfields (at the circumferential locations) within the compressor are decoupled in the circumferential direction, in actuality they are coupled non-axisymmetrically

through the body force $\vec{f}$. As will be seen in the next section, the pressure change associated with the inertia of the fluid within the rotor (in relative motion) and the flow redistribution through the compressor (e.g. due to upstream flow nonuniformities) will act to couple the local flowfields at the circumferential positions non-axisymmetrically. Thus, this representation of the compressor (or blade) can be referred to as an unsteady non-axisymmetric actuator duct model.

5.3 Compressor Modelling

As alluded to in Section 5.1, we will confine ourselves to the application of the overall methodology to the situation of low speed, multi-stage compressors. Thus, the compressor pressure rise and the relevant Mach numbers are assumed to be low enough so that compressibility effects can be considered negligible. However, the compressor hub-to-tip ratio can be low so that there is a need to account for the effects due to three-dimensionality of the flow in the compressor model.

In contrast to high hub-to-tip ratio compressors, low hub-to-tip ratio compressors have essentially three geometrical length scales: compressor circumference, blade span, and blade pitch. The inclusion of the blade span length scale within the compressor model means that the spanwise (i.e. radial) distribution of flow properties through the compressor must be considered. For instance, the spanwise distribution of flow properties across a blade row can be modified as a result of (i) the radial movement of the streamsurface, and (ii) the deformation/twist in the streamsurfaces due to the development of secondary flow within the blade passage (see Fig. 4).

The development of secondary flow within a blade passage can be a result of flow nonuniformities (either externally imposed or self-induced) upstream of the compressor or blade row. The resulting streamsurface deformation due to secondary flow can alter the pitchwise average value, and hence the spanwise distribution of the flow properties. Such a redistribution of flow properties can impact the spanwise distribution of flow properties of subsequent blade rows. This is a three-dimensional flow effect and constitutes a coupling between the blade pitch length scale and the blade span length scale nonuniformities (such as that associated with a radial

variation). Thus, the compressor pressure rise under these flow conditions can be considered to consist of the axisymmetric flow performance (such as that determined from a well-correlated streamline curvature code) and a correction to account for the redistribution of flow properties associated with flow three-dimensionality (such as that resulting from streamsurface deformation due to secondary flow in a blade passage). In Section 5.3.1 we present the development of a methodology to compute such a correction to the compressor axisymmetric performance.

When the blade rows are subjected to flow unsteadiness, there is a non-steady flow effect due to the acceleration (or deceleration) of the fluid within the blade passages, even if the blade passage flowfield responds in a quasi-steady manner. This acceleration (or deceleration) of fluid requires an unsteady pressure difference across the blade rows, and hence the compressor [6]. The compressor pressure rise in unsteady flow thus consists of the axisymmetric flow performance corrected for flow redistribution associated with three-dimensional flow effect and a correction to account for the quasi-steady response of the compressor to flow unsteadiness. In Section 5.3.2 we will describe how this unsteady pressure difference is calculated within the framework of the overall methodology as presented in Section 5.1.

The compressor can be assumed to respond quasi-steadily only if the length scale of the unsteady flowfield disturbances are of the order of the compressor circumference (i.e. disturbances with low order circumferential harmonic), and the associated reduced frequency is low. However, when the unsteady disturbances are such that their spectral content contains high circumferential harmonics (i.e. equivalently high reduced frequency), the blade pressure losses and the flow angle deviation at exit of the blade rows will respond unsteadily (rather than quasi-steadily). These aspects of the compressor response will be examined in Section 5.3.3.

5.3.1 Flow Redistribution Due to Three-Dimensional Effects

The compressor pressure rise characteristics and the flowfield based on the axisymmetric flow performance can be calculated using a *well-correlated* streamline curvature code (i.e. one that has been developed and used in an engine company). The compressor (axisymmetric) flowfield

computed by the streamline curvature code will be known as the primary flow. For the situation where the compressor is subjected to a radially non-uniform flow, the flow redistribution due to the radial movement of the axisymmetric streamsurfaces through the compressor can be determined from the streamline curvature code. The flow redistribution due to the streamsurface deformation/twist associated with the secondary flow development in the blade passage, however, cannot be assessed nor computed using the streamline curvature code.

A way to get this information would be the direct application of a 3-D Euler flow solver, but such an approach, though feasible, would be relatively demanding in terms of computational resources for a multi-stage compressor within the framework of the approach presented in Section 5.1. In view of this, a model (to be described in the following) was developed to allow the assessment and calculation of flow redistribution in the compressor as a result of radial nonuniformities. As will be seen later, the usefulness of the model is examined by comparing the computed results against those from a standard 3-D flow solver; the key idea behind the flow model is that the three-dimensional flow can be approximated by the superposition of the secondary flow on the primary flow. The primary flow can be determined by the streamline curvature method as described in the above, and the secondary flow can be calculated based on the concept of classical secondary flow theory [12] - [14].

As the effects associated with the radial movement and the deformation of streamsurfaces are of an inviscid nature and are not due to compressibility effects, the flow model was developed based on the inviscid and incompressible assumption (compressibility effects can readily be included if warranted). The flow model was then used to elucidate the three-dimensional flow effect on the flow redistribution for a stator blade passage, a rotor blade passage, and a three-stage compressor.

5.3.1.1 Radial Movement of Axisymmetric Streamsurfaces

The radial movement of the axisymmetric streamsurfaces through a compressor annulus is governed by the radial equilibrium equation, which essentially expresses a dynamic balance

between pressure gradient and the acceleration due to streamline curvature. The equations for radial equilibrium and the continuity condition can be readily solved using the standard streamline curvature technique [15]. The inviscid assumption adopted here implies that viscous effects are not included. Thus, the main mechanism responsible for the radial movement of the streamsurfaces considered here is the two-dimensional blade pressure rise coefficient, C_p:

$$C_p = \frac{P_{exit} - P_{inlet}}{\frac{1}{2}\rho V_{inlet}^2} = \left(1 - \frac{\cos^2 \alpha_{inlet}}{\cos^2 \alpha_{exit}}\right) \tag{3}$$

where subscripts "inlet" and "exit" pertain to the respective values at the blade inflow and outflow planes, α denotes the flow angle, V_{inlet} the inlet velocity, and ρ the density.

To illustrate this qualitatively, consider the flow situation in Fig. 4a; the static pressure rise along a streamtube is determined by its area ratio change between the blade passage inlet and exit, i.e.

$$P_{exit} - P_{inlet} = \frac{1}{2}\rho V_{inlet}^2 \left[1 - \left(\frac{A_{inlet}}{A_{exit}}\right)^2\right] \tag{4}$$

where A denotes the streamtube cross-sectional area. For the same area ratio, the low stream would therefore yield a lower pressure rise than the high flow one due to the lower inlet dynamic head.

Thus, the streamsurface moves in a direction to result in an increased area ratio for the low flow stream and hence an increased pressure rise. Correspondingly, there would also be a decreased area ratio for the high flow stream so that there is a larger velocity defect at the passage exit than at the inlet. Thus, the amount of radial shift in the streamsurface is essentially determined by the pressure rise coefficient as well as the strength and the extent of inlet flow nonuniformities. It should also be noted that any loss associated with viscous effects will also affect the pressure distribution (hence the pressure rise across the blade row) and thus the radial movement of the streamsurface; this can be included in the model based on appropriate loss correlations (such loss correlations are included in streamline curvature codes used in the gas turbine industry).

5.3.1.2 Streamsurface Deformation/Twist

The deformation of the streamsurface within a blade passage (see Fig. 4b) is a result of the development of secondary flow through the blade passage [12] - [14]. It is thus possible to evaluate the flow redistribution due to this effect by using techniques developed for secondary flow problems in turbomachinery (i.e. the secondary flow approximation). This would necessitate the development of a procedure (see Section 5.3.1.3) to determine the extent of the twist in the streamsurfaces in terms of the streamwise vorticity generated in the blade passage. The streamwise vorticity can be developed, for instance, as a result of the turning of the normal vorticity at the inlet (due to flow nonuniformities) into the streamwise direction. A general expression for the generation of streamwise vorticity [12] - [14] is

$$\left(\vec{W}\cdot\nabla\right)\left(\frac{\vec{W}\cdot\vec{\omega}}{W^2}\right)=-\left(\frac{\vec{W}\times\nabla\rho}{\rho}\right)\cdot\left[\frac{\left(\vec{W}\cdot\nabla\right)\vec{W}+2\vec{\Omega}\times\vec{W}+\vec{\Omega}\times\left(\vec{\Omega}\times\vec{W}\right)}{W^2}\right] \qquad (5)$$

$$+2\left[\frac{\vec{W}\times\left(\vec{\omega}\times\vec{W}\right)}{W^2}\right]\cdot\frac{\left(\vec{W}\cdot\nabla\right)\vec{W}}{W^2}-\frac{2\left(\vec{\omega}\times\vec{W}\right)\cdot\vec{\Omega}}{W^2}$$

where the relative velocity $\vec{W}$ is related to the absolute velocity $\vec{V}$ and the rotor angular velocity $\vec{\Omega}$ via

$$\vec{W}=\vec{V}-\vec{\Omega}\times\vec{r}\ .$$

The absolute vorticity $\vec{\omega}$ is $\nabla\times\vec{V}$. The LHS of the equation is the change of (ω_s/W_s) (where subscript "s" denotes the streamwise component) along a streamline and is a result of the generation of streamwise vorticity ω_s. The first term on the RHS of Eq. (5) is a result of density nonuniformity, the second term a result of the turning of the flow through the blade passage, and the last term a result of Coriolis acceleration. It is useful to note that the vector product $\vec{\omega}\times\vec{W}$ appearing in the second term on the RHS of (5) can be expressed in terms of the gradient of rotary stagnation pressure, P_t^*, and density, ρ, as

$$\vec{\omega}\times\vec{W}=-\frac{\nabla P_t^*}{\rho}+\left(\frac{1}{2}W^2-\frac{1}{2}r^2\Omega^2\right)\frac{\nabla\rho}{\rho} \qquad (6)$$

Equation (5) can be integrated along a nominal streamline on the streamsurfaces deter-

mined from the streamline curvature calculation procedure (i.e. the primary flow); this yields an estimate of the streamwise vorticity distribution on a cross-flow plane from which the associated secondary flow can be computed from a (secondary flow) streamfunction ψ that satisfies

$$\nabla^2\psi = -(\omega_s + \bar{\omega}_s) \tag{7}$$

where $\bar{\omega}_s$ is the computed streamwise vorticity from the streamline curvature procedure, while ω_s is computed from Eq. (5).

In computing the flow redistribution due to streamsurface deformation at blade trailing edge plane, a further simplification is adopted as indicated below. Equation (5) is integrated to give an estimate of the streamwise vorticity distribution at the blade passage exit; Eq. (7) is then solved for the associated secondary flowfield on the inlet and exit of the passage. A linear combination may then be taken between the inlet and the exit to yield an approximation of the secondary flow development through the blade passage. The resulting velocity, which consists of this secondary flow superimposed upon the primary flow, may next be used to determine the extent of streamsurface deformation at the passage exit. The soundness of this simplification is assessed by comparing the results against those from a standard 3-D flow solver.

In the next section, we summarize the procedure based upon the flow module in Sections 5.3.1.1 and 5.3.1.2 for computing the flow redistribution through the compressor.

5.3.1.3 Computational Procedure

Given the compressor's geometrical configuration and the flowfield at an axial location upstream of the compressor face, the following procedures are carried out:

1) Use the streamline curvature procedure to compute the primary flowfield through a blade row;
2) Compute the absolute vorticity from the streamline curvature solution;
3) Compute the streamwise vorticity at the inlet to the blade passage;
4) Compute the streamwise vorticity at the passage exit by integrating Eq. (5) from inlet to exit along streamlines determined in the streamline curvature solution from step (1) above;
5) Compute the secondary flow at the inlet and exit by solving for the secondary flow

streamfunction ψ from Eq. (7);

6) Estimate the secondary flow development through the blade passage based on the approximation presented in Section 5.3.1.2;
7) Compute the streamsurface deformation by tracking particle paths from blade leading edge to trailing edge plane based on a flowfield that consists of secondary flow (as determined in step (6)) superposed on the primary flow (as determined in step (1));
8) Determine the redistribution of flow properties (e.g. ρ, P_t, P_t^*, etc.) from the streamline curvature solution and a knowledge of the deformed streamsurfaces in step (7);
9) Compute the pitchwise averages of the velocity and flow properties from the results in step (8); and
10) Repeat steps (1) to (9) for all subsequent blade rows in the compressor.

The above procedure yields a methodology for computing the steady-state performance of a compressor subjected to an incoming spanwise distortion in stagnation pressure and temperature. This computational procedure has been coded in a computer program module for the case of inviscid and incompressible flow. A simple steady-loss model based on Howell's loss correlation [16] has been included in the computational module. In the incompressible limit, a measure of the temperature distortion can be in terms of density nonuniformity. A well-correlated streamline curvature code can be used in step (1) above instead of the rudimentary streamline curvature procedure coded here. If a well-correlated streamline curvature code from industry is used in step (1) above, then compressibility effects would be accounted for in the axisymmetric flow performance.

In the next section, representative examples from the computations based on the flow model described here will be presented for: (i) illustrating the extent of flow redistribution; and (ii) comparison against results from a standard flow solver.

5.3.1.4 Representative Examples

Approximations have been introduced in the development of the computational model for

calculating flow redistribution in a compressor subjected to upstream flow nonuniformities. As the flow effects considered are of an inviscid nature, it is thus appropriate to assess the goodness of the model by comparison against three-dimensional Euler calculations [17], [18]. A typical result of such a comparison for a rotor blade row is shown in Fig. 5. The rotor, with a hub-to-tip ratio of 0.8, has an inlet blade angle of 45° and an outlet blade angle of 20° (this corresponds to a blade pressure rise coefficient of 0.45), and is subjected to a 2:1 tan*h* inlet shear in the axial velocity profile (Fig. 6); the rotor speed is chosen to maintain flow incidence near to zero so that the solution would be representative of an inviscid one.

As shown in Fig. 5, the contours of rotary stagnation pressure at the passage exit calculated by the model and a 3-D Euler solver agree both in terms of the deformation and the radial movement of the streamsurfaces (the discrepancy in the results on the blade surfaces is most likely due to numerical diffusion inherent in the Euler code). This is also reflected in the good agreement of the pitchwise-average spanwise profile of stagnation pressure at the blade passage exit, shown in Fig. 7, predicted by the model and the 3-D Euler solver. The results of Fig. 7 also show the three-dimensional flow effect on the redistribution of stagnation pressure at the exit where the spanwise profile predicted by the model is distinctly different from that based on the streamline curvature prediction. Though not shown here, a similar trend on redistribution of stagnation pressure at exit is observed when the rotor is subjected to a 2:1 tan*h* shear in density. (Note that it would not be necessary to consider the effect of density nonuniformities for stator passages since the Munk and Prim [19] flow substitution principle may be used to substitute nonuniform density flows by nonuniform velocity flows with the same streamlines and total pressure distribution.)

Parametric studies that have been carried out based on the model have indicated the following:

i) the spanwise movement of the streamsurfaces depends on the blade static pressure rise coefficient (i.e. blade loading) and the spanwise flow nonuniformities; and

(ii) the importance of the deformation of streamsurfaces due to streamwise vorticity is determined

by the ratio of blade pitch to blade span; for low values of this ratio, the effect is localized while for values comparable to 1, the twisting of streamsurfaces affects the entire passage flow.

As an illustration, the model has also been used to calculate the axisymmetric pressure rise across a three-stage compressor (Fig. 8a) for: (i) uniform upstream flow, and (ii) upstream flow with spanwise nonuniformity. When a simple loss model based on Howell's correlation [16] is incorporated into the computational model for computing the axisymmetric pressure rise across the three-stage compressor for (i) uniform upstream flow, and (ii) upstream flow with spanwise nonuniformity, the corresponding results are displayed in Fig. 8b. These computed results indicate that, when the compressor is subjected to upstream flow with spanwise variation, the flow redistribution associated with 3-D flow effects acts to degrade the performance. No attempt has been made to validate these against experimental data. However, if a well-correlated streamline curvature code is used instead, the computed pressure rise characteristics can be expected to have quantitative reliability.

In summary, we have demonstrated the validity and usefulness of the model to compute flow redistribution through multi-stage compressors in a practical manner. The flow redistribution due to radial movement and deformation of streamsurfaces produces a change in the spanwise profile of flow properties; this can be interpreted as a radial mixing effect [20], [21] which results in a coupling among short circumferential length scale, finite blade pitch and radial variation in the flowfield.

The significance of flow redistribution through the compressor due to three-dimensional flow effects has to be assessed in terms of the impact it has on the compressor stability margin and performance in distorted flow. This can only be examined when the compressor model is integrated with the upstream and downstream flowfield.

5.3.2 Pressure Rise Correction Due to Flow Unsteadiness

This pressure rise correction arises out of the requirement of a non-steady pressure

difference to balance the acceleration of the fluid in the blade row. Portions of this unsteady pressure rise correction are computed directly through the solution of Eqs. (1) and (2) for the entire flowfield. However, the portion associated with the acceleration of fluid in a rotor blade row in relative motion to spatial flow nonuniformities needs to be modelled and accounted for in the approach delineated in Section 5.1. Following the exposition in Refs. [6] and [7], this additional correction can be obtained using

$$(\Delta P)_{inertia} = \vec{S}_{inertia} = \lambda \frac{\partial \vec{V}}{\partial \theta} \tag{7}$$

where $\vec{V} = (U\hat{e}_r, V\hat{e}_\theta, W\hat{e}_z)$

and $\lambda = \dfrac{C_x}{r \cos^2 \xi}$

with C_x as the axial chord length, ξ as the blade stagger angle, and $(\hat{e}_r, \hat{e}_\theta, \hat{e}_z)$ denoting the unit vector in the cylindrical coordinate system (r,θ,z).

As with the influence of flow redistribution, this inertia force term acts to couple non-axisymmetrically the local axisymmetric flowfield described by Eq. (2) at each circumferential position. Thus, for flow nonuniformities involving circumferential variation, the inertia force within the compressor can be calculated as follows:

1) Compute the compressor flowfield at a set of preselected circumferential locations;
2) Evaluate the acceleration vector given by the product of angular velocity and the gradient of velocity vector in the circumferential direction. This is directly proportional to the inertia force;
3) Advance to the next time step, allowing for the relative motion between compressor blade row and flow nonuniformity given by the product of relative angular velocity and the differential time step; and
4) Repeat steps (1) to (3).

5.3.3 Effect of Unsteady Loss and Deviations on Compressor Performance in Distorted Flow

In the work reported in Refs. [8] - [10], the compressor is assumed to respond in a quasi-

steady manner. However, experimental data has indicated that when the compressor is subjected to an inlet distortion, the instantaneous flow quantity (e.g. loss, deviation) lags the steady state due to a delayed boundary layer response to changes in incidence; the time τ for the boundary layer to respond scales with the time it takes for a fluid particle to traverse through the blade passage. Haynes et al. [25], Mazzawy [22] and Nagano [23] suggested the use of a lag law to model the unsteady losses and unsteady deviations which display such a hysteresis effect. The lag law reasonably predicts the unsteady blade response to incidence as shown in Fig. 9.

In the light of the above, the effects of the compressor unsteady response on compressor performance in distorted flow have been examined during the course of this research program. This work is fully documented in Ref. [24]. While aspects of the effect of compressor unsteady response were examined based on an extension of the two-dimensional flow model presented in [8] - [10], nevertheless the results should provide useful guidelines on inclusion of relevant aspects of unsteady response in the three-dimensional flow model for compressors in distorted flow.

In the calculations and results reported in Ref. [24], the unsteady response of the compressor are described by the first order lag law as follows:

$$\tau_{loss} \frac{\partial}{\partial t} \text{Loss} = (\text{Loss})_{steady} - \text{Loss} \tag{8a}$$

$$\tau_{deviation} \frac{\partial}{\partial t} \beta_{exit} = (\beta_{exit})_{steady} - \beta_{exit} \tag{8b}$$

where the flow angle β is measured in the relative frame.

We summarize below the results of stability calculations with unsteady response of a compressor, as described by the first order lag law of Eq. (8), in distorted flow:

i) Compressor instability occurs at higher distorted pressure rise and lower flow coefficients compared to that based on the quasi-steady response of the compressor;

ii) With a first order lag model for unsteady loss and deviations (Eq. (8)), eigenmodes with the strongest harmonic content greater than the first harmonic are stabilized; thus as shown in Fig. 10 when subjected to a single-lobed distortion, the first harmonic goes unstable first, followed by the second, the third, etc.;

iii) Inclusion of unsteady deviations and unsteady loss appears to have a greater impact on the stability margin of compressors that are swirl sensitive.

We conclude this subsection by presenting the comparison (Fig. 11) between the calculated and measured propagation and growth rates for small amplitude flowfield disturbances undertaken by Haynes et al. [25] for a three-stage compressor. By an appropriate choice of the time constant τ_{loss} (~1.5 x convection time), the growth rates and propagation speed for the first three modes appeared to be well predicted across a range of flow coefficients; however, non-steady deviation appears to have a negligible effect for this case. In summary, a simple first order lag model for unsteady loss appears to capture the effects of unsteady response of the compressor; such a model was used for 3-D linearized stability calculations presented in Section 6.0.

5.3.4 Summary on Compressor Modelling

The procedures presented in Sections 5.3.1 to 5.3.3 essentially provide one with a rational method of computing the body force distribution $\vec{f}$ that represents the action of the compressor on the flowfield. The modified streamline curvature procedure with flow redistribution due to three-dimensional flow effects yields (f_r, f_θ, f_z) (or alternatively (f_r, f_z) and pitchwise-averaged tangential velocity (V) distribution) without the inertia force distribution due to acceleration of fluid in the rotor blade passage; the latter is computed by the procedure of Section 5.3.2. Additional correction due to unsteady flow and deviation discussed in Section 5.3.3 can be included in the values of $\vec{f}$ and V. However, in order to reliably generate the compressor characteristics (and hence the body force distribution without the inertia force distribution), one may need the use of a well-correlated streamline curvature code (such as reside in the aircraft engine companies).

5.4 Numerical Techniques

In this section, we briefly describe the numerical technique for the solution of Eqs. (1) and (2). The state vector $\vec{U}$ is modified to

$$\vec{U} = \begin{bmatrix} \frac{1}{C^2} rP \\ rU \\ rV \\ rW \end{bmatrix}$$

so that one can apply the standard numerical technique for unsteady 3-D Euler solver to the solution of unsteady inviscid incompressible flow equations. The term $\frac{1}{C^2}\frac{\partial rP}{\partial t}$ appearing in the continuity equation is known as the pseudo-compressibility effect. In the limit of steady-state flow, the steady inviscid incompressible flow equations are recovered. As we are interested in the time-accurate solution, the numerics and the choice of C^2 must be such as to maintain time accuracy as well as the relevant frequency wave number information of the disturbance flow field. A four-stage Runge-Kutta time-stepping scheme is chosen for advancing Eqs. (1) and (2) in time, and spatial discretization is based on a finite volume procedure. Fluxes of flow variables across a cell face, A, is evaluated according to

$$\text{Flux across A} = \text{Area of A} \times \tfrac{1}{2}(F_{j+1} + F_j)$$

and if cell face A is between upstream (downstream) and compressor inlet (exit), then for $W > 0$:

$$\text{Flux across A} = \text{Area of A} \times \tfrac{1}{2}(1.5\, F_j + 0.5\, F_{j-1})$$

and for $W < 0$:

$$\text{Flux across A} = \text{Area of A} \times \tfrac{1}{2}(F_{j+1} + F_j)$$

The numerics and the choice of C^2 were evaluated to ensure that the requirements for time-accuracy and pertinent frequency wave number relation are satisfied.

The approach presented here has been implemented in an executable computer program for an engine compression system shown in Fig. 3. For convenience of reference, it will be referred to as the Integrated Flowfield Computational Model (IFCM). The assessment of the IFCM against known analytical results from Refs. [6] - [8] will be presented in the next section.

5.5 An Assessment of the Present Approach

The integrated flowfield computational model (IFCM) has been applied to the computation of the response of a multi-stage compressor to inlet distortion. The approach can be assessed by

comparing the results against known analytical results presented in Refs. [6], [7], and [8]. The two-dimensional version of IFCM was used to compute the response of a compressor subjected to a far upstream square wave distortion with a circumferential extent of 180 degrees. As the results in Fig. 12 show, the compressor inlet flow coefficient distribution from this calculation was in good agreement with that from the two-dimensional analytical model of Ref. [8]. Next, the three-dimensional version of IFCM was used to compute the response of a compressor, with a high hub-to-tip ratio of 0.9, to a far upstream distortion identical to the one above. The flow coefficient distributions at the hub, the midspan location, and the shroud from this calculation are shown in Fig. 13; not only do the results indicate the near-absence of any spanwise variation but they are also in good agreement with the two-dimensional results from Ref. [8].

The above diagnostic calculations are not exhaustive, but they nevertheless yield computed results that are in agreement with known analytical solutions from Ref. [8]. However, the proposed approach has the potential of being far more general in application to three-dimensional flow situations. As an illustration, the three-dimensional version of the IFCM has been used to compute the response of a low hub-to-tip ratio (0.4) compressor subjected to a purely circumferential flow nonuniformity of the square wave type at a far upstream location. The compressor is assumed to have a pressure rise characteristic that is invariant radially. Both the two-dimensional and three-dimensional versions of the IFCM have been used to compute the distorted pressure rise characteristic as the compressor is throttled towards the stall point; these computed results are shown in Fig. 14 up to the stability limit (or stall point) indicated in the figure. Solutions at or past the point of stability limit exhibit unsteady behavior in that no steady solution can be obtained. These calculations have been implemented to demonstrate the potential of the present proposed approach. The results of Fig. 14 give an initial glimpse of the influence of three-dimensionality on stability margin, even though it is small for the flow situation being computed here. Again, the computed results presented so far are for incompressible flow, but extension to the high speed regime is conceptually straightforward and direct.

It was stated above that when the integrated flowfield computational model (IFCM) was

used to compute the compressor response (to distorted flow) past the stability limit, the solution exhibited unsteady behavior. As the method is time-accurate, such solution behavior can be exploited to compute the temporal and spatial (nonlinear) evolution of the compressor flowfield instabilities of various types (one-dimensional, two-dimensional, as well as three-dimensional). This aspect of the IFCM was assessed by its application to the computation of flow instabilities in a compression system with uniform upstream flow for comparisons against known 2-D results in Refs. [6], [7], and [26]. As the results in Table 1 show, the growth rate and phase speed of the flowfield disturbance computed using IFCM are in good agreement with the analytical results from the 2-D linearized stability analysis. The computed results in Fig. 15 show the evolution of incipient flow instability into the final stall cell pattern with characteristics similar to those presented in Ref. [26].

In summary, the good agreement between the IFCM results and known two-dimensional results for the compressor response to inlet distortion and flow instability development in uniform flow can be viewed as an indication of a high level of confidence in the proposed conceptual approach.

6.0 Analysis of Three-Dimensional Flow Instabilities in Compressors

The two-dimensional model of Refs. [6] - [9] applies to situations of compressor instabilities and the response of the overall compression system to circumferential distortion where a 2-D flow assumption is valid. A key development in the work is the use of rigorous linear stability analysis techniques, which have been widely used to advantage in classical hydrodynamic stability problems, to address the stability issues. It would be useful to adopt such an approach for investigating fluid dynamic stability of radially non-uniform axisymmetric flow through a highly-loaded fan (e.g. that of ADP) or a compressor subjected to a general unsteady, non-axisymmetric disturbance. The background flow, being axisymmetric but radially non-uniform, can be appropriately calculated using a streamline curvature technique, for example.

The major task in this effort consisted of developing a procedure that is computationally

efficient for assessing the stability of the unsteady, non-axisymmetric (and three-dimensional) disturbance; this could amount to the efficient solution of an eigenvalue problem with the eigenvalues corresponding to the growth rate of the imposed disturbance field.

To obtain a general description (i.e. a description to an arbitrary mean background flow in a representative compressor annulus) it was decided that the most useful approach was to cast the formulation in terms of the primitive variables (i.e. through velocity components and the pressure for incompressible flow). Such a formulation for the three-dimensional stability analysis of flow in terms of the primitive variables will be presented in Section 6.1. In Section 6.2, implementation of the stability calculations that involve the numerical solution of a three-dimensional eigenvalue problem formulated in Section 6.1 is described. As in Section 5.0, the technique for the stability calculation developed here was assessed by comparing the computed results against two-dimensional results from Refs. [6] - [9] and analytical solutions for three-dimensional rectilinear cascades. The results of these comparisons are presented in Section 6.3. We then use the technique to examine the influence of flow three-dimensionality on compressor stability and the spectral content of the marginally stable flow disturbance field.

6.1 Formulation of the 3-D Linearized Stability Calculation

The radially non-uniform axisymmetric flow in the compressor annulus (Fig. 16) is represented by the velocity field ($\bar{U}(r,z)$, $\bar{V}(r,z)$, $\bar{W}(r,z)$) and the pressure field $\bar{P}(r,z)$; this flow can be computed using a streamline curvature approach. To examine the fluid dynamic stability of this flowfield to a general unsteady, non-axisymmetric disturbance ($u(r,\theta,z,t)$, $v(r,\theta,z,t)$, $w(r,\theta,z,t)$, $p(r,\theta,z,t)$), we first linearize this disturbance flow about the background axisymmetric flow to give, for the upstream, downstream, and blade-gap flowfields,

Continuity Equation:

$$\frac{1}{r}\frac{\partial}{\partial r}(ru) + \frac{1}{r}\frac{\partial v}{\partial \theta} + \frac{\partial w}{\partial z} = 0 \tag{9}$$

Momentum Equation:

$$\frac{\partial u}{\partial t} + \bar{U}\frac{\partial u}{\partial r} + u\frac{\partial \bar{U}}{\partial r} + \frac{\bar{V}}{r}\frac{\partial u}{\partial \theta} + \bar{W}\frac{\partial u}{\partial z} + w\frac{\partial \bar{U}}{\partial z} = -\frac{\partial p}{\partial r} + \frac{2\bar{V}v}{r} \tag{10a}$$

$$\frac{\partial v}{\partial t} + \frac{\bar{U}}{r}\frac{\partial rv}{\partial r} + \frac{u}{r}\frac{\partial r\bar{V}}{\partial r} + \frac{\bar{V}}{r}\frac{\partial v}{\partial \theta} + \bar{W}\frac{\partial v}{\partial z} + w\frac{\partial \bar{V}}{\partial z} = -\frac{\partial p}{\partial \theta} \tag{10b}$$

$$\frac{\partial w}{\partial t} + \bar{U}\frac{\partial w}{\partial r} + u\frac{\partial \bar{W}}{\partial r} + \frac{\bar{V}}{r}\frac{\partial w}{\partial \theta} + \bar{W}\frac{\partial w}{\partial z} + w\frac{\partial \bar{W}}{\partial z} = -\frac{\partial p}{\partial z} \tag{10c}$$

where the flow variables are appropriately made non-dimensional in terms of the compressor tip speed, a characteristic tip radius r_t^*, and the density ρ. The disturbance flow satisfying the above linearized equations are subjected to the boundary conditions: (i) specified across the compressor or each blade row of the compressor; (ii) that the velocity component normal to the hub and the casing of the compressor annulus should vanish identically; and (iii) far upstream and far downstream are such that the flow disturbances must at all times have their physical origin at the compressor. The boundary conditions across the compressor involve the linking of the disturbance flowfields (external to the compressor or blade rows) across the compressor (or each of the blade rows) to enforce the conservation of mass, momentum, and specified (geometrical) constraints on flow path; these boundary conditions reflect the dynamics of the compressor response presented in Section 5.3. As such, the explicit expressions for the compressor boundary conditions depend upon the details of the flow model for the compressor or blade row (see Sections 6.2 and 6.3).

The disturbance flow can be conveniently expressed in the form of:

$$\begin{bmatrix} u(r,\theta,z,t) \\ v(r,\theta,z,t) \\ w(r,\theta,z,t) \\ p(r,\theta,z,t) \end{bmatrix} = \sum_{n=-\infty}^{n=\infty} \begin{bmatrix} u_n(r,z) \\ v_n(r,z) \\ w_n(r,z) \\ p_n(r,z) \end{bmatrix} e^{in\theta}\, e^{i\omega_n t} = \sum_{n=-\infty}^{n=\infty} \vec{u}_n(r,z)\, e^{in\theta}\, e^{i\omega_n t} \tag{11}$$

where we have used the notation

$$\vec{u}_n(r,z) = \begin{bmatrix} u_n(r,z) \\ v_n(r,z) \\ w_n(r,z) \\ p_n(r,z) \end{bmatrix}$$

Substitution of Eq. (11) in Eqs. (9) and (10) gives, upon invoking the orthogonality condition for the Fourier series in $e^{in\theta}$,

$$A(r,z)\frac{\partial \vec{u}_n}{\partial r} + B(r,z)\frac{\partial \vec{u}_n}{\partial z} + C(r,z)\,\vec{u}_n + D(\omega)\,\vec{u}_n = 0 \tag{12}$$

where

$$A = \begin{bmatrix} 1 & 0 & 0 & 0 \\ \bar{U}(r,z) & 0 & 0 & 1 \\ 0 & \bar{U}(r,z) & 0 & 0 \\ 0 & 0 & \bar{U}(r,z) & 0 \end{bmatrix}$$

$$B = \begin{bmatrix} 0 & 0 & 1 & 0 \\ \bar{W}(r,z) & 0 & 0 & 0 \\ 0 & \bar{W}(r,z) & 0 & 0 \\ 0 & 0 & \bar{W}(r,z) & 1 \end{bmatrix}$$

$$C = \begin{bmatrix} \frac{1}{r} & \frac{in}{r} & 0 & 0 \\ \left[\frac{\partial \bar{U}}{\partial r} + \frac{in}{r^2}(r\bar{V})\right] & -\frac{2}{r^2}(r\bar{V}) & \frac{\partial \bar{U}}{\partial z} & 0 \\ \frac{1}{r}\frac{\partial}{\partial r}(r\bar{V}) & \left[\frac{\bar{U}}{r} + \frac{in}{r^2}(r\bar{V})\right] & \frac{1}{r}\frac{\partial r\bar{V}}{\partial z} & \frac{in}{r} \\ \frac{\partial \bar{W}}{\partial r} & 0 & \left[\frac{\partial \bar{W}}{\partial z} + \frac{in}{r^2}(r\bar{V})\right] & 0 \end{bmatrix}$$

$$D(\omega) = \begin{bmatrix} 0 & 0 & 0 & 0 \\ i\omega & 0 & 0 & 0 \\ 0 & i\omega & 0 & 0 \\ 0 & 0 & i\omega & 0 \end{bmatrix}$$

Likewise, the use of Eq. (11) allows the boundary conditions across the compressor (or each of the blade rows at $z = z_\ell$) to be written as

$$c(r,z_\ell)\,\vec{u}_n^{\,*} + d(\omega)\,\vec{u}_n^{\,*} = 0 \tag{13}$$

where we have represented the compressor (or each of the blade rows) as an actuator disk at $z = z_\ell$. The coefficients $c(r,z_\ell)$, and $d(\omega)$ depend on the details of the flow model for the compressor; the specific form of these coefficients will be explicitly delineated in Sections 6.2 and 6.3. In Eq. (13), $\vec{u}_n^{\,*}(r,z_\ell)$ is given as

$$\vec{u}_n^* = \begin{bmatrix} \vec{u}_n^-(r,z_\ell) \\ \vec{u}_n^+(r,z_\ell) \end{bmatrix} \tag{14}$$

where superscripts "-" and "+" denote values evaluated immediately upstream and downstream of the actuator disk.

In examining the stability of the disturbance flow $\vec{u}(r,\theta,z,t)$ for a given steady axisymmetric background flow, we seek a disturbance flow that can marginally be sustained subject to the boundary conditions across the compressor, far upstream and far downstream, along the hub and casing of the compressor annulus. Mathematically, this amounts to the determination of compressor operating conditions for which a disturbance flow $\vec{u}$ with a ω that has a vanishing imaginary part. As we shall see later, this is tantamount to the solution of an eigenvalue problem with the eigenvalue ω corresponding to the growth rate of the unsteady non-axisymmetric (and three-dimensional) disturbance flow.

6.2 A Numerical Technique for the Differential Eigenvalue Problem

In this section, we present a numerical method for the determination of eigenvalues (ω) of the system of partial differential equations (i.e. Eqs. (12) and (13)) that govern the unsteady non-axisymmetric disturbance flow. As a Fourier series has been used to represent the θ-dependence of the flow, we need only to define a two-dimensional grid on the radial-axial (r-z) plane for a discrete approximation to the derivatives $\partial/\partial r$ and $\partial/\partial z$. We have applied a standard second-order central finite difference approximation away from the boundary and a one-sided finite difference approximation for a normal derivative at points along the boundary. Upon substituting these finite difference approximations for the various derivatives in Eqs. (12) and (13), we obtain a matrix eigenvalue problem of the form

$$A\vec{\chi} + i\omega B\vec{\chi} = 0 \tag{15}$$

where the eigenvalues ω and the eigenvector

$$\vec{\chi} = \begin{bmatrix} \vec{u}_n^u\left(r_j, z_k\right) \\ \vec{u}_n^d\left(r_j, z_k\right) \end{bmatrix} = \begin{bmatrix} \vec{u}_{njk}^u \\ \vec{u}_{njk}^d \end{bmatrix} \tag{16}$$

can be determined using a standard algorithm for the solution of the matrix eigenvalue problem. In Eq. (16), subscript "jk" denotes the value at grid point (j,k) on the radial-axial plane, and superscripts "u" and "d" denote the value upstream and downstream of the actuator disk representing the compressor. The matrices A and B contain information on the state of the background axisymmetric flow, geometry of the compressor annulus, compressor design characteristics (such as pressure rise characteristics, number of stages, etc.), dynamics of the compressor response, and characteristics of any other components making up the compression system. Physically, the eigenvector $\vec{\chi}$ provides information on the structure of the flow disturbance (i.e. the eigenmodes of the compression system) while the eigenvalue ω (which has a real part and an imaginary part) describes the growth rate and phase speed of the corresponding eigenmode $\vec{\chi}$. Such an analytical procedure would thus provide us with a technique for establishing a direct link between the 3-D instability inception process and the compressor characteristics.

In the next section, we apply the above solution technique to the 3-D stability analysis of flow in specific flow situations through a compressor with specific design characteristics.

6.3 Computed Results from Instability Analysis

The 3-D linearized stability calculation procedure was first assessed by comparisons against known two-dimensional analytical results [6] and analytical solutions for three-dimensional rectilinear cascades. As the background axisymmetric flow far upstream of the compressor is taken to be uniform in these cases, the upstream disturbance flow can be simply described in terms of a perturbations potential $\phi(r,\theta,z,t)$ instead of the primitive variables. The boundary conditions applied are then as follows:

a) continuity condition:

$$\frac{\partial \phi^-}{\partial z} = w^+ \tag{17}$$

b) blades exert no radial force :

$$\frac{\partial \phi^-}{\partial r} = u^+ \tag{18}$$

c) momentum condition (i.e. pressure rise condition):

$$p^+ - p^- = \frac{\partial \bar{\psi}}{\partial W} w^\pm - \lambda \left(\frac{\partial w}{\partial \theta}\right)^\pm - \mu \left(\frac{\partial w}{\partial t}\right)^\pm \tag{19}$$

where $\bar{\psi}$ denotes the axisymmetric compressor pressure rise characteristic, λ the unsteady blade response parameter for rotor blades, and μ the unsteady blade response parameter for both stator and rotor blades.

d) compressor exit angle condition:

$$v^+ = (\tan \beta_{exit})\, w^+ \tag{20}$$

e) at a far upstream location:

$$\frac{\partial \phi}{\partial z} = 0 \tag{21a}$$

f) at a far downstream location:

$$\frac{\partial p}{\partial z} = 0 \tag{21b}$$

The boundary conditions in Eqs. (17) to (20) can be cast into the form shown in Eq. (13).

The results of the comparisons between the present numerical matrix eigenvalue solver and the analytical solutions are shown in Fig. 17, Table II and Table III. Figure 17 shows the comparison of computed flow variables from the present technique against those from the two-dimensional analytical results, while the results of Tables II and III show the computed eigenvalues against those obtained analytically for two-dimensional cascades and three-dimensional rectilinear cascades. The three-dimensional flow disturbance in a rectilinear cascade has a circumferential harmonic, denoted by n, which is coupled to the spanwise spectral content (denoted by j). Thus, each eigenmode in the three-dimensional stability calculation for the rectilinear cascade is characterized by a circumferential harmonic n and a radial harmonic j. The results shown in Table II are for n = 1 and j = 1, 2, 3, 4. These comparisons, though limited,

indicate the good agreement between the results obtained by the present numerical technique and those from known analytical solutions, and serve to impart confidence in the numerical solution procedure based on the theoretical formulation of Sections 6.1 and 6.2.

We now present the results from a 3-D stability calculation for a rotor-stator combination stage. For a background flow with uniform axial velocity in the spanwise direction and a slope of stage pressure rise characteristic that is invariant from the hub to the tip, stability calculations were carried out to examine the dependence of instability onset on the radial spectral content of the modal flow disturbance. The computed results for this situation, displayed in Fig. 18, indicate that the modes corresponding to non-zero n but j = 0 (i.e. the two-dimensional modal disturbances analogous to those in [6] - [10], [26]) become marginally unstable at a flow coefficient for which the total-to-static pressure rise characteristics have zero slope. However, for modal flow disturbances that have a circumferential as well as radial harmonic content (i.e. genuinely three-dimensional modal flow disturbance), they become marginally unstable at flow coefficients for which the total-to-static pressure rise characteristics have a positive slope. When the slope of the stage pressure rise characteristics is allowed to vary from hub to tip, as indicated in Fig. 19, the computed results of Fig. 20 show that the flow disturbances can become marginally unstable at flow coefficients for which the radially-averaged slope of the characteristics is still negative. This is the first instance that such an effect is predicted based on a theoretical analysis/computation.

The effect of unsteady loss on the instability onset was assessed by inclusion of a loss model based on the simple first order lag law presented in Section 5.3.3. This modifies the pressure rise condition in Eq. (19) to

$$p^+ - p^- = \frac{\partial \bar{\Psi}_i}{\partial \bar{W}} w - \ell_R - \ell_S - \lambda \frac{\partial w}{\partial \theta} - \mu \frac{\partial w}{\partial t} \tag{22}$$

where the loss ℓ_R associated with the rotor is given as

$$\tau_R \left(\frac{\partial \ell_R}{\partial t} + \frac{\partial \ell_R}{\partial \theta} \right) = \frac{\partial L_R}{\partial W} w - \ell_R \tag{23a}$$

while the loss ℓ_S associated with the stator is given as

$$\tau_S \frac{\partial \ell_S}{\partial t} = \frac{\partial L_S}{\partial W} w - \ell_S \qquad (23b)$$

with L_R and L_S denoting the quasi-steady loss characteristics for the rotor and the stator, and Ψ_i the ideal compressor characteristics The computed results based on the above simplistic loss model show a trend similar to that seen in the two-dimensional results presented in Section 5.3.3.

6.4 Summary of 3-D Linearized Stability Analysis

We now summarize the results from the limited 3-D linearized stability calculations that have been implemented so far:

i) the three-dimensional equivalence of the two-dimensional modes (i.e. those eigenmodes with nonzero n but zero p) become unstable first;

ii) the radial structure of the modal flow disturbance depends on the variation of the slope of the characteristics with radius;

iii) compressor instability onset can occur on the negative slope (radially-averaged) of the compressor characteristics for the situation where the slope of the pressure rise characteristics varies from hub to tip;

iv) there is a difference between the instability onset for a three-dimensional flowfield and that obtained from a 2-D stability calculation based on the radially-averaged compressor characteristics.

7.0 CONCLUDING REMARKS ON THE STATUS OF PREDICTIVE CAPABILITY FOR 3-D FLOW INSTABILITIES IN COMPRESSORS

When the research program was initiated in 1989, the analysis/computational tools for examining compressor flow stability were confined to low speed compressors in situations where the two-dimensional flow assumption would be approximately valid; this necessarily implies that the compressor has a high hub-to-tip ratio where flow redistribution (within the compressor) can be considered to be negligible. Furthermore, in the solution methods reported in [6] - [10] and [26], the disturbance flowfield upstream of the compressor is taken to be a two-dimensional irrotational one linearized about the background flow, while that downstream of the compressor is

determined by the two-dimensional linearized Euler equations.

When the research program was concluded in 1993, we had the computational tools to provide us with the capability for addressing three-dimensional stability issues in low hub-to-tip ratio compressors. These include: (1) a 3-D linearized stability computational procedure for assessing the stability of a steady, radially nonuniform, axisymmetric flow through a compressor to a general 3-D unsteady flow disturbance; and (2) a 3-D, nonlinear, computational technique for computing the temporal and spatial nonlinear development of aerodynamic instabilities in a compression system (Fig. 3) in situations where the compressor is subjected to an incoming uniform flow as well as to an externally imposed or self-induced flow distortion of the 3-D type. The accomplishments achieved in the research program are best summarized in Table IV, which assesses the current status of compression system modelling against that in 1989.

The completed work in (1) and (2) above constitute a significant advancement in the methodologies for computing the inception and development of 3-D flow instabilities in compressors operating in uniform as well as nonuniform flow. The availability of these computational tools will provide us with the opportunity to now focus more on the key technical issues of technological interests rather than on the development and modelling issues for the methodologies. Thus, while the research program was initially focused on problems associated with the development of VSTOL engines, it also resulted in the defining of an overall conceptual approach and the developing of the necessary computational methodologies for examining technical issues associated with compression system instabilities on a long-term basis. Extension of the approach and methodologies for investigation of instabilities in high speed compressors is direct and straightforward.

References

1. Williams, D.D., 1984, "Inlet-Engine Compatibility: Part I--Total Pressure Distortion; Part II-Other Forms of Intake Flow Distortion," Short Course - Workshop Engine-Airframe Integration, Bangalore, India.

2. Day, I.J., 1993, "Stall Inception in Axial Flow Compressors," *ASME J. of Turbomachinery*, Vol. 115, pp. 1-9.

3. Longley, J. etc., 1994, "Effects of Rotating Inlet Distortion on Multistage Compressor Stability" to be presented at ASME 1994 Conference.

4. McDougall, N.M., Cumpsty, N.A., and Hynes, T.P., 1990, "Stall Inception in Axial Compressors," *ASME J. of Turbomachinery*, Vol. 112, pp. 116-125.

5. Garnier, V.H., Epstein, A.H., and Greitzer, E.M., 1991, "Rotating Waves as a Stall Inception Indication in Axial Compressors," *ASME J. of Turbomachinery*, Vol. 113, pp. 290-302.

6. Moore, F.K., 1983, "A Theory of Rotating Stall of Multistage Axial Compressors: Parts I, II & III," *ASME J. of Engineering for Gas Turbines and Power*, Vol. 106.

7. Moore, F.K., Greitzer, E.M., 1985, "A Theory of Post-Stall Transients in Axial Compression Systems, Parts I, II," *ASME J. of Engineering for Gas Turbines and Power*, Vol. 108.

8. Hynes, T. P., and Greitzer, E. M., 1987, "A Method for Assessing Effects of Inlet Distortions on Compressor Stability," *ASME J. of Turbomachinery*, Vol. 109.

9. Chue, R., Hynes, T., Greitzer, E.M., Tan, C.S., and Longley, J.P., 1989, "Calculations of Inlet Distortion Induced Compressor Flow Field Instability," *Int. J. of Heat and Fluid Flow*, Vol. 10.

10. Longley, J.P., 1988, "Inlet Distortion and Compressor Stability," Ph.D Thesis, Engineering Department, Cambridge University.

11. Adamczyk, J., 1985, "Model Equations for Simulating Flows in Multistage Turbomachinery", ASME Paper 85-GT-226.

12. Hawthorne, W.R., 1955, "The Growth of Secondary Circulation in Frictionless Flow," *Proc. Cambridge Philosophical Society*, Vol. 51, Part 4, pp. 737-743.

13. Squire, H.B., Winter, K.G., 1951, "The Secondary Flow in a Cascade of Airfoils in a Nonuniform Stream," *J. of the Aeronautical Sciences*, pp. 271-277.

14. Smith, L.H., 1953, "Three-Dimensional Flow in Axial-Flow Turbomachinery, Part I: Theoretical Determinatino of Secondary Flow," *Internal Flow Research*, Report I-14, Johns Hopkins University.

15. Novak, R., 1967, "Streamline Curvature Computing Procedures for Fluid Flow Problems," *ASME J. of Eng. for Power*, Vol. 89, pp. 478-490.

16. Howell, A.R., 1942, "The Present Basis of Axial Flow Compressor Design, Part I: Cascade Theory and Performance," ARC R&M 2095.

17. Adamczyk, J.J., Celestina, M.L., Beach, T.A., Garnett, M., 1989, "Simulation of Three-Dimensional Viscous Flow Within a Multi-Stage Turbine," *ASME J. of Turbomachinery*, Vol. 112, No. 3, pp. 370-376.

18. Denton, J.D., 1985, "The Calculation of Fully Three Dimensional Flow Through Any Type of Turbomachinery Blade Row," AGARD LS 140, 3-*D Computation Techniques Applied to Internal Flows in Propulsion Systems.*

19. Munk, M., Prim, R., 1947, "On the Multiplicity of Steady Gas Flows Having the Same Streamline Pattern," *Proc. Nat. Acad. Sciences*, Vol. 33, pp. 137-141.

20. Adkins, G.G., Smith, L.H., 1982, "Spanwise Mixing in Axial Flow Turbomachines," *ASME J. of Eng. for Power*, Vol. 104, pp. 97-110.

21. Gallimore, S.J., Cumpsty, N.A., 1986, "Spanwise Mixing in Multistage Axial Flow Compressors, Parts I & II," *ASME J. of Turbomachinery*, Vol. 108, pp. 2-16.

22. Mazzawy, R.S., 1977, "Multiple Segment Parallel Compressor Model for Circumferential Flow Distortion," *ASME J. of Eng. for Power*, Vol. 99, pp. 228-246.

23. Nagano, ??, Machida, S., Takata, H., 1971, "Dynamic Performance of Stalled Blade Rows," Japan Society of Mech. Engineers Paper JSME-11, presented at Tokyo Joint International Gas Turbine Conference, pp. 73-80.

24. Strang, E., 1991, "Influence of Unsteady Losses and Deviations on Compression System Stability with Inlet Distortion," M.S. Thesis, MIT Dept. of Aeronautics and Astronautics.

25. Haynes, J.M., Hendricks, G.J., Epstein, A.H., 1993, "Active Stabilization of Rotating Stall in a Three-Stage Axial Compressor," ASME Paper 93-GT-346, presented at 1993 ASME Gas Turbine Conference, Cincinnati, OH.

26. Chue, R., Greitzer, E.M., Tan, C.S., 1987, "An Analysis of General Post-Stall Transients in Axial Compression Systems," unpublished GTL research work.

TABLE I
GROWTH RATE AND PHASE SPEED OF INCIPIENT INSTABILITY

	Present ICFM Results	2-D Analytical Results
Growth Rate	0.253	0.259
Phase Speed	0.274	0.270

TABLE II
NUMERICALLY DETERMINED EIGENVALUES VS. ANALYTICAL EIGENVALUES FOR A 2-D FLOW SITUATION IN A COMPRESSOR

Analytic Eigenvalue	Numerically Determined Eigenvalues
-0.3887 – 0.6478 i	-0.3893 – 0.6488 i

TABLE III
NUMERICALLY DETERMINED EIGENVALUES VS. ANALYTICAL EIGENVALUES FOR A FLOW SITUATION IN 3-D RECTILINEAR CASCADES

– Results Shown for First 4 Radial Modes
Correponding to Circumferential Harmonic of 1 –

Radial Mode	Analytical	Numerically Determined
0th	-0.2222 – 0.1389 i	-0.2213 – 0.1383 i
1st	-0.4719 + 0.2936 i	-0.4719 + 0.2918 i
2nd	-0.4855 + 0.3031 i	-0.4856 + 0.2962 i
3rd	-0.4902 + 0.3062 i	-0.4904 + 0.2961 i

TABLE IV
COMPRESSION SYSTEM MODELLING IN 1989 VS. 1993

COMPRESSION SYSTEM MODELLING (1989)

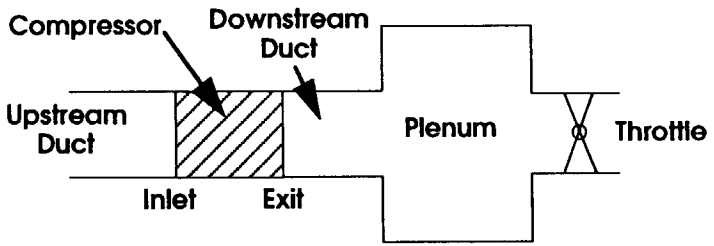

- Upstream/downstream flow field models
  - 2-D linearized Euler equations (upstream irrotational)
  - Analytic solution upstream and downstream
  - Axial mean flow upstream (or with circumferential distortion)
- Compressor model
  - Low speed
  - High hub-to-tip ratio
  - No internal redistribution

COMPRESSION SYSTEM MODEL NOW

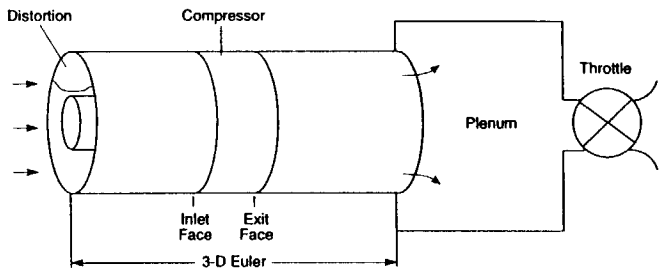

- Upstream and downstream: 3-D Euler solver (nonlinear and rotational)
- Compressor: compressor characteristic specified as a function of r or body-force distribution (with effects of flow redistribution)
- Low hub-to-tip compressor
- Plenum
- Throttle

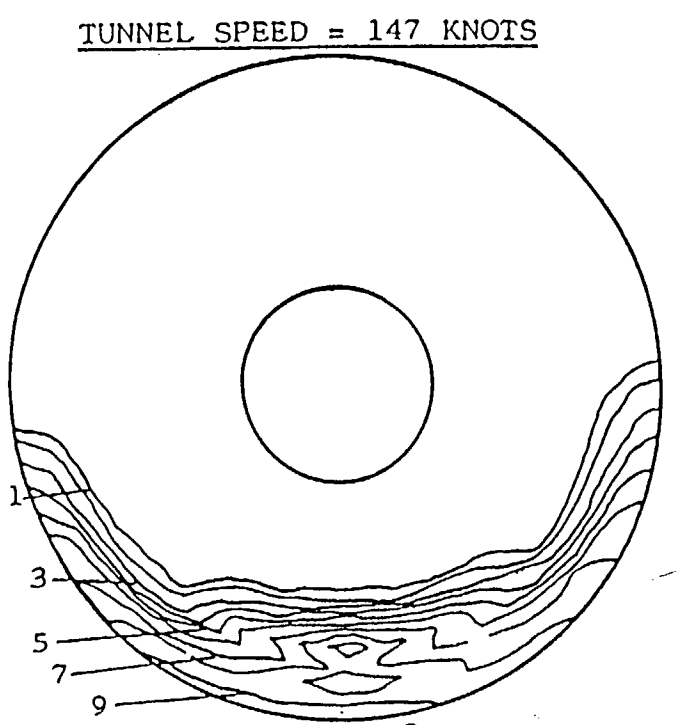

Figure 1a

LOCAL TOTAL
PRESSURE RECOVERY

1	0.99
2	0.98
3	0.96
4	0.94
5	0.92
6	0.90
7	0.86
8	0.82
9	0.78
0	0.74

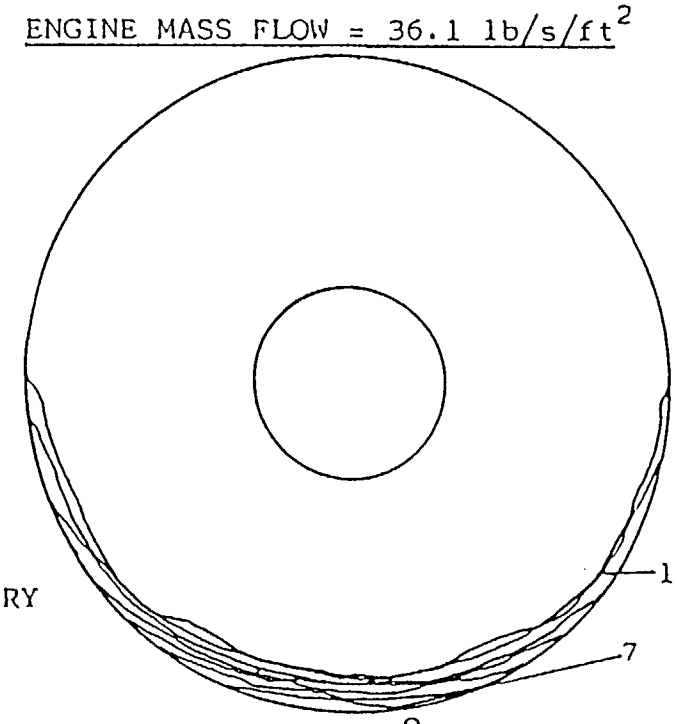

Figure 1b

Fig. 1: An inlet tested at incidence both without and with the aeroengine interaction. The fluid dynamic coupling between the two components has a strong effect on the flow distribution [1].

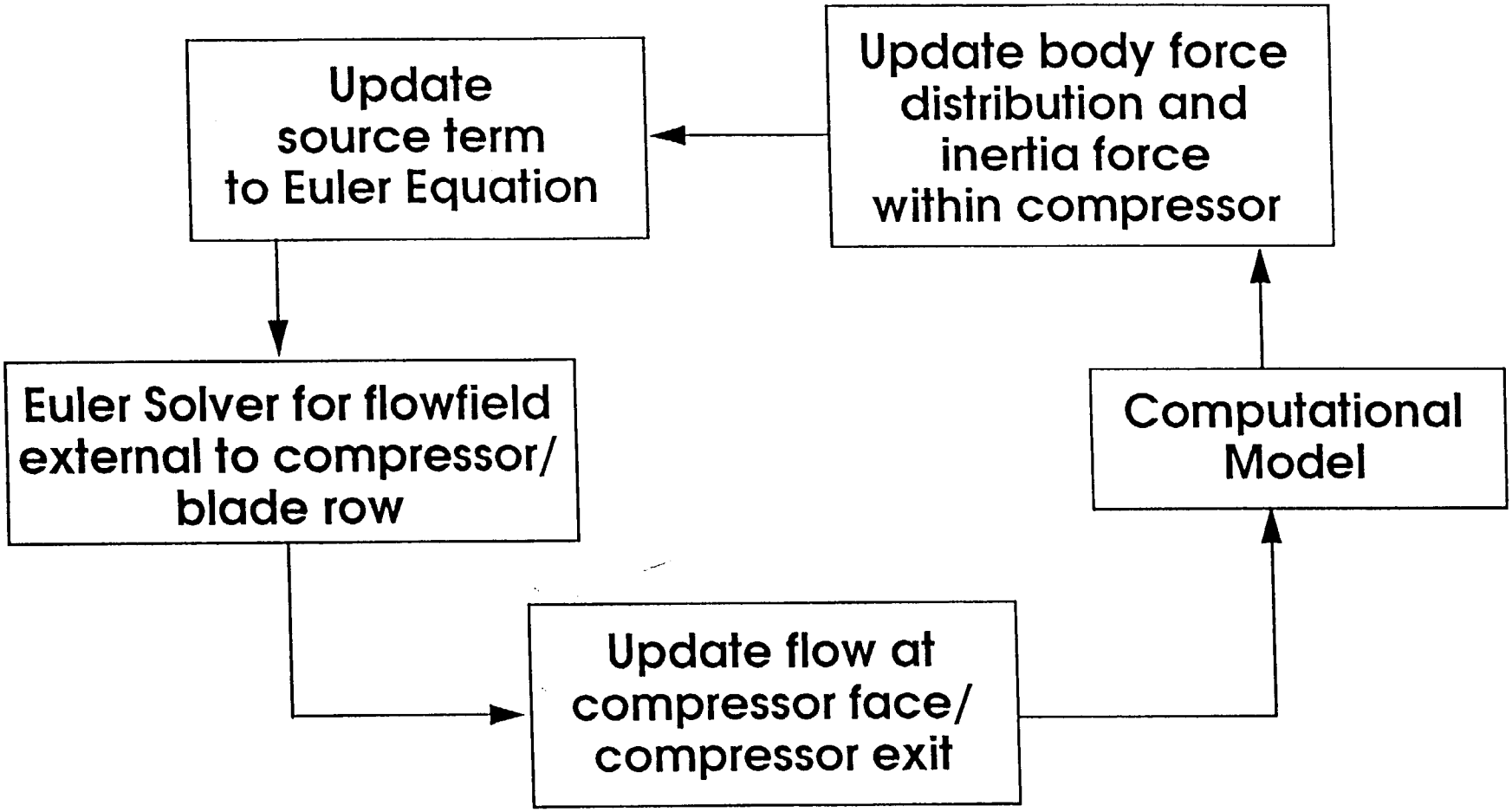

Fig. 2: Overall conceptual approach for computing the response of a compressor to distorted flow and the evolution of compressor instabilities.

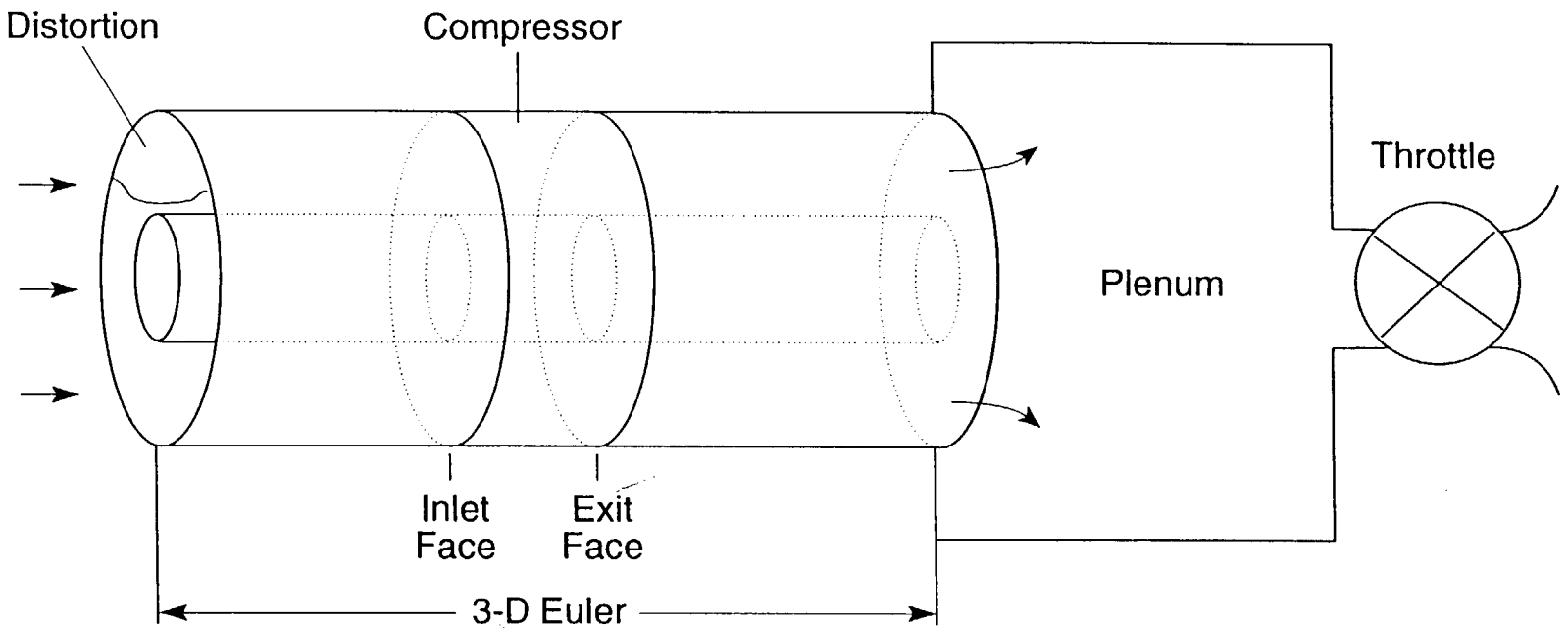

Fig. 3: A general compression system model.

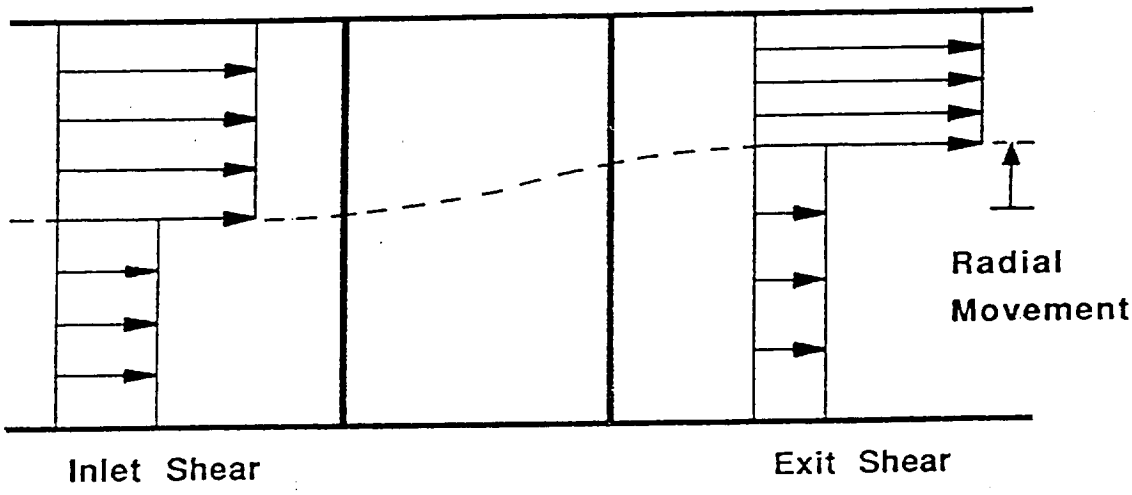

Fig.4a: An illustration of radial movement of the streamsurface: radial movement of a shear layer through a stator passage occurs to achieve the required matching pressure rise.

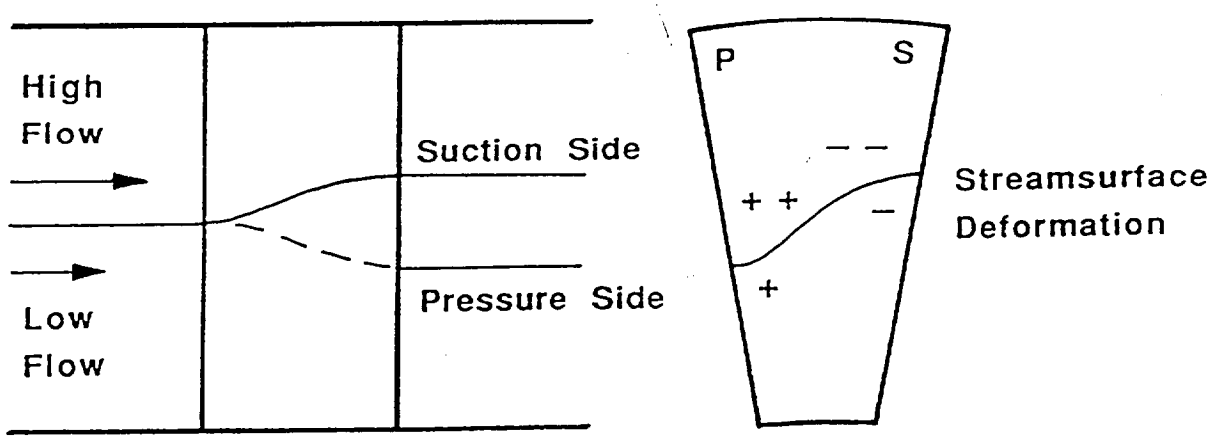

Fig.4b: An illustration of twist in the streamsurface: a shear layer through a stator passage deforms due to secondary flow. The cross-passage pressure gradients are larger in the high flow stream (upper portion) and the resulting pressure imbalance causes the streamsurface to twist.

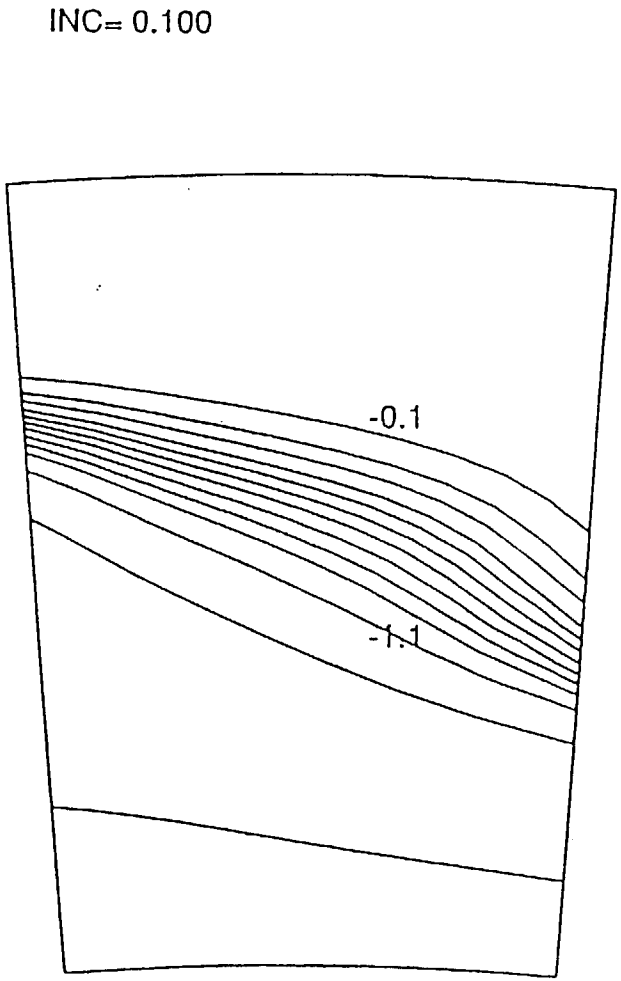

Fig. 5a: Contours of rotary stagnation pressure from the computational model.

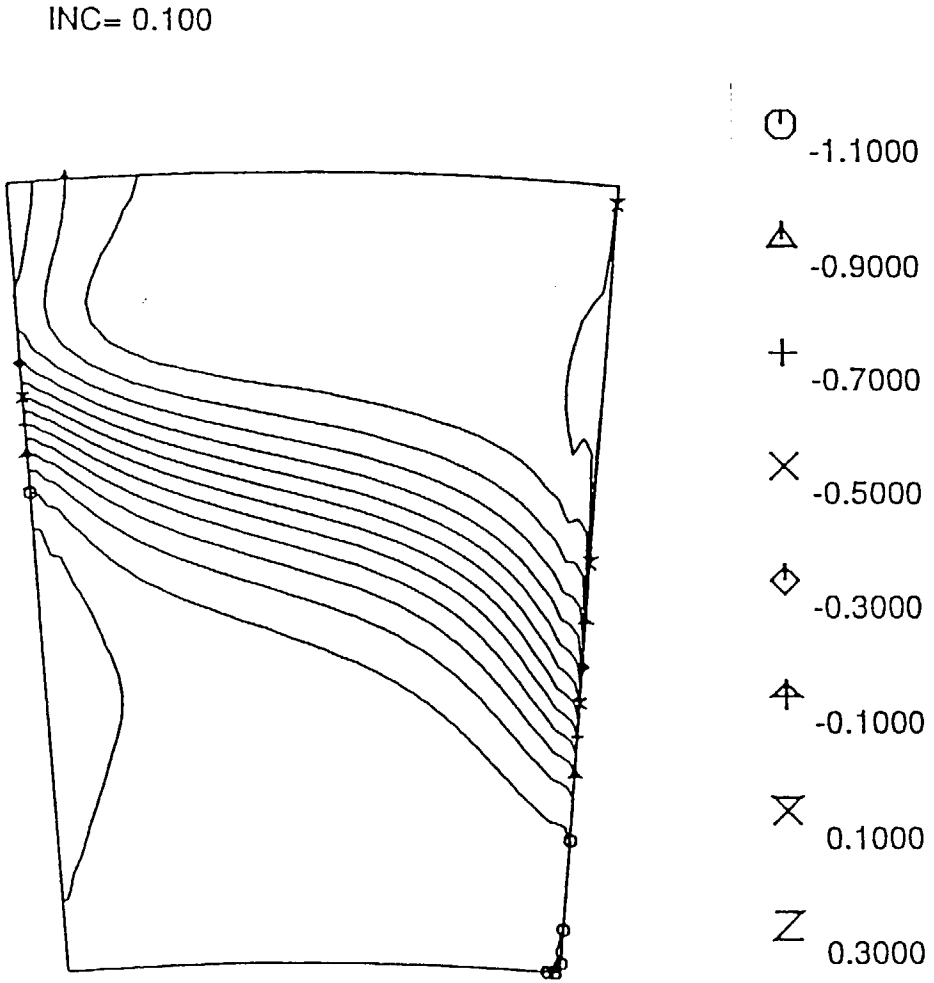

Fig. 5b: Contours of rotary stagnation pressure from the 3-D Euler calculation [17].

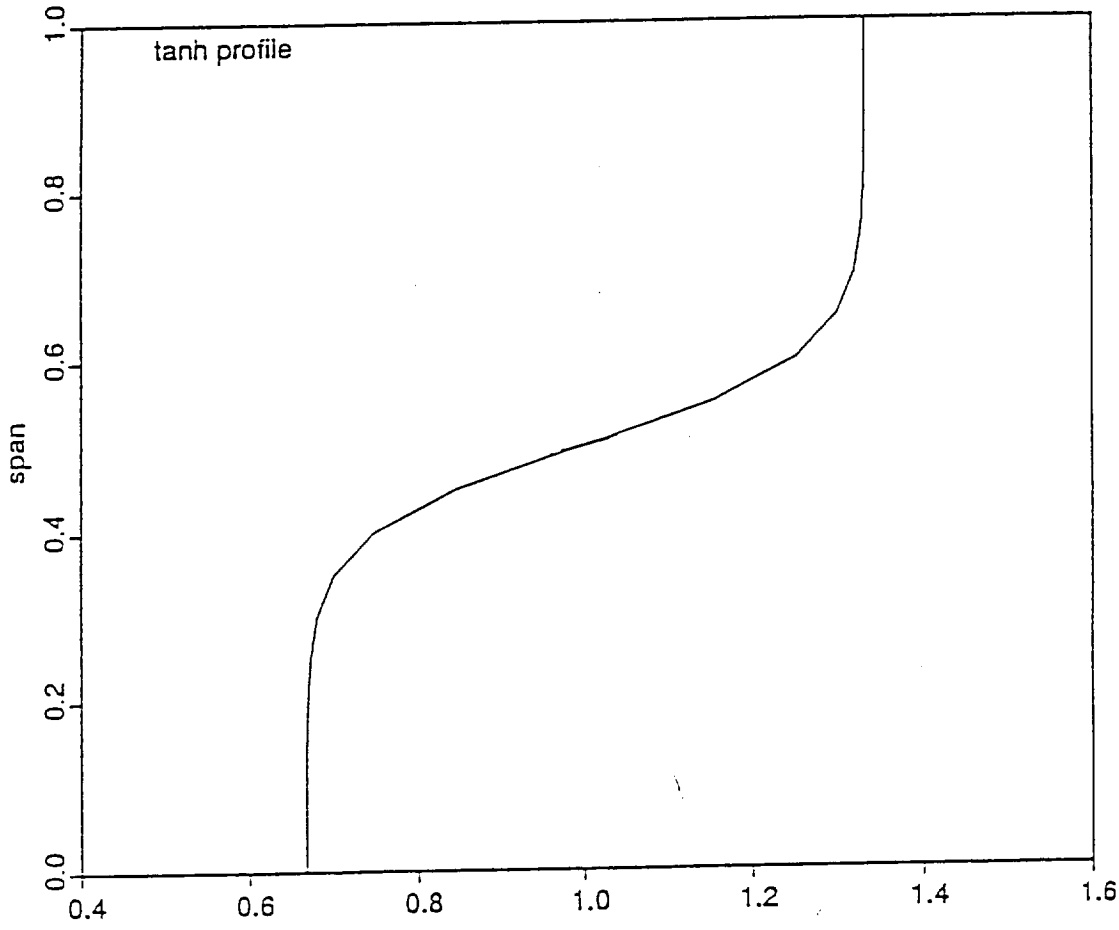

Fig.6: A 2:1 tan*h* profile.

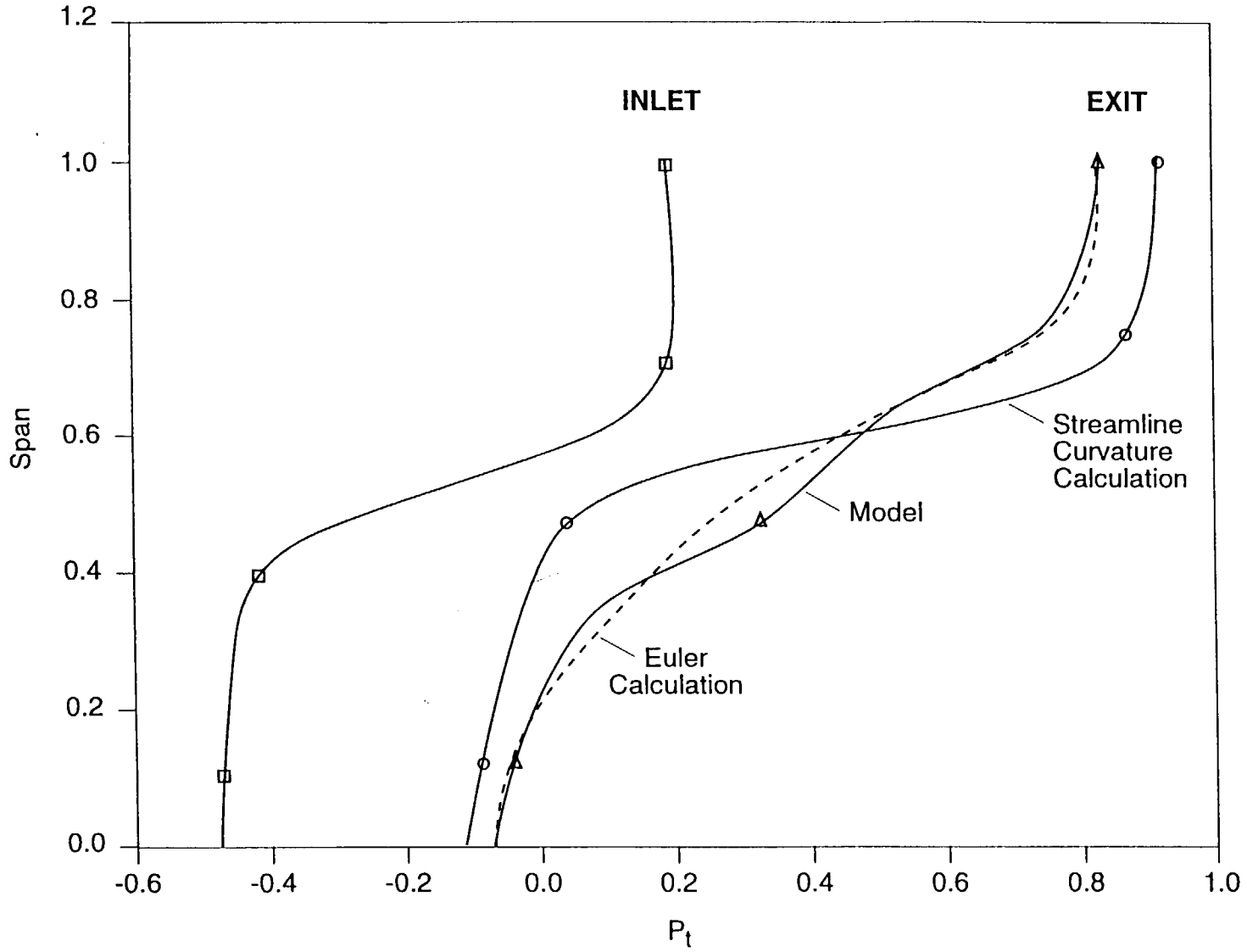

Fig. 7: Stagnation pressure distribution calculated by the model and the Euler calculation.

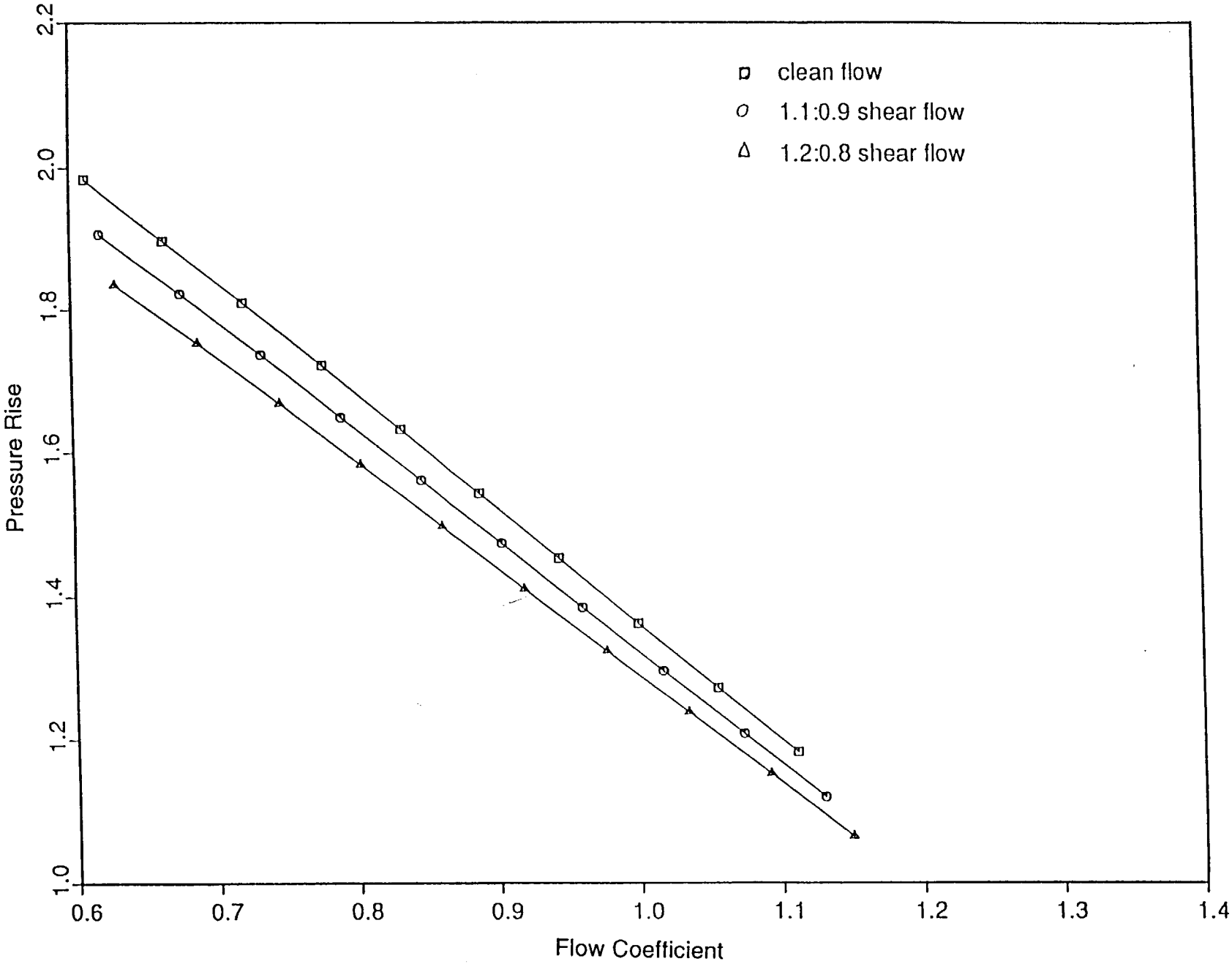

Fig. 8a: Ideal (no loss) axisymmetric pressure rise for a 3-stage compressor with upstream uniform flow and upstream flow with spanwise non-uniformity.

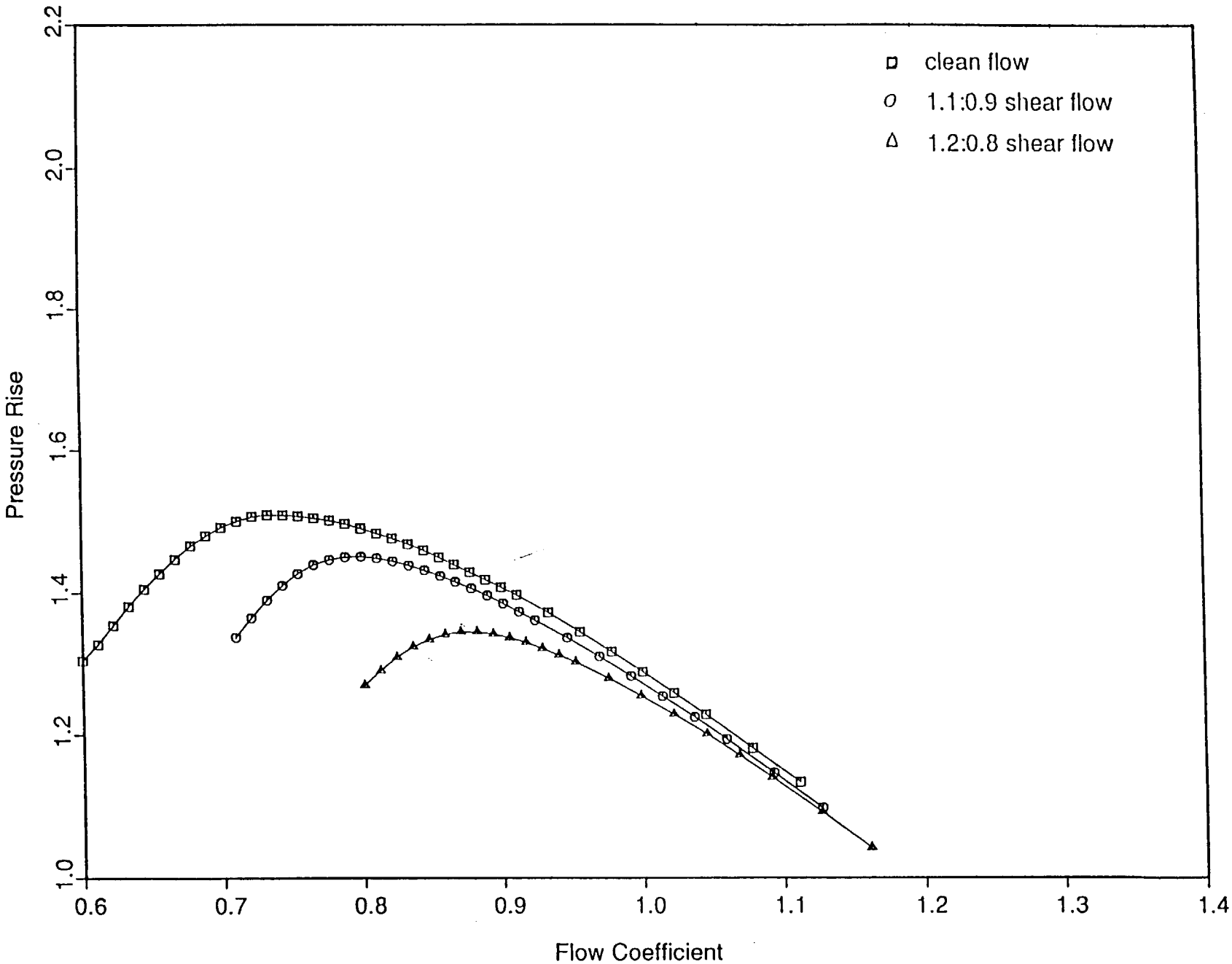

Fig. 8b: Axisymmetric pressure rise with a simple loss model based on Howell's correlation [16].

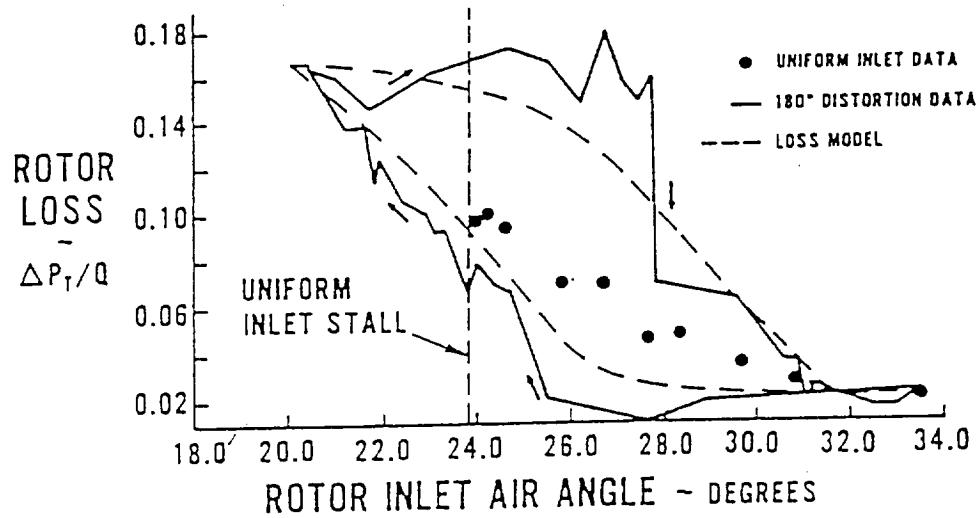

Fig.9a: Loss coefficient as a function of incidence.

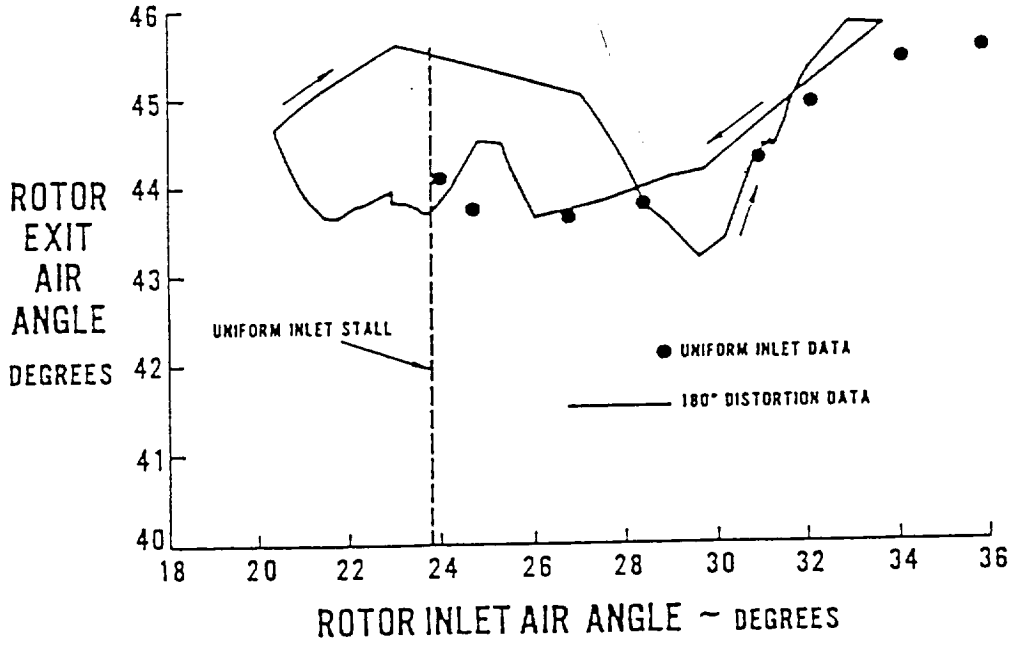

Fig.9b: Blade deviation as a function of incidence.

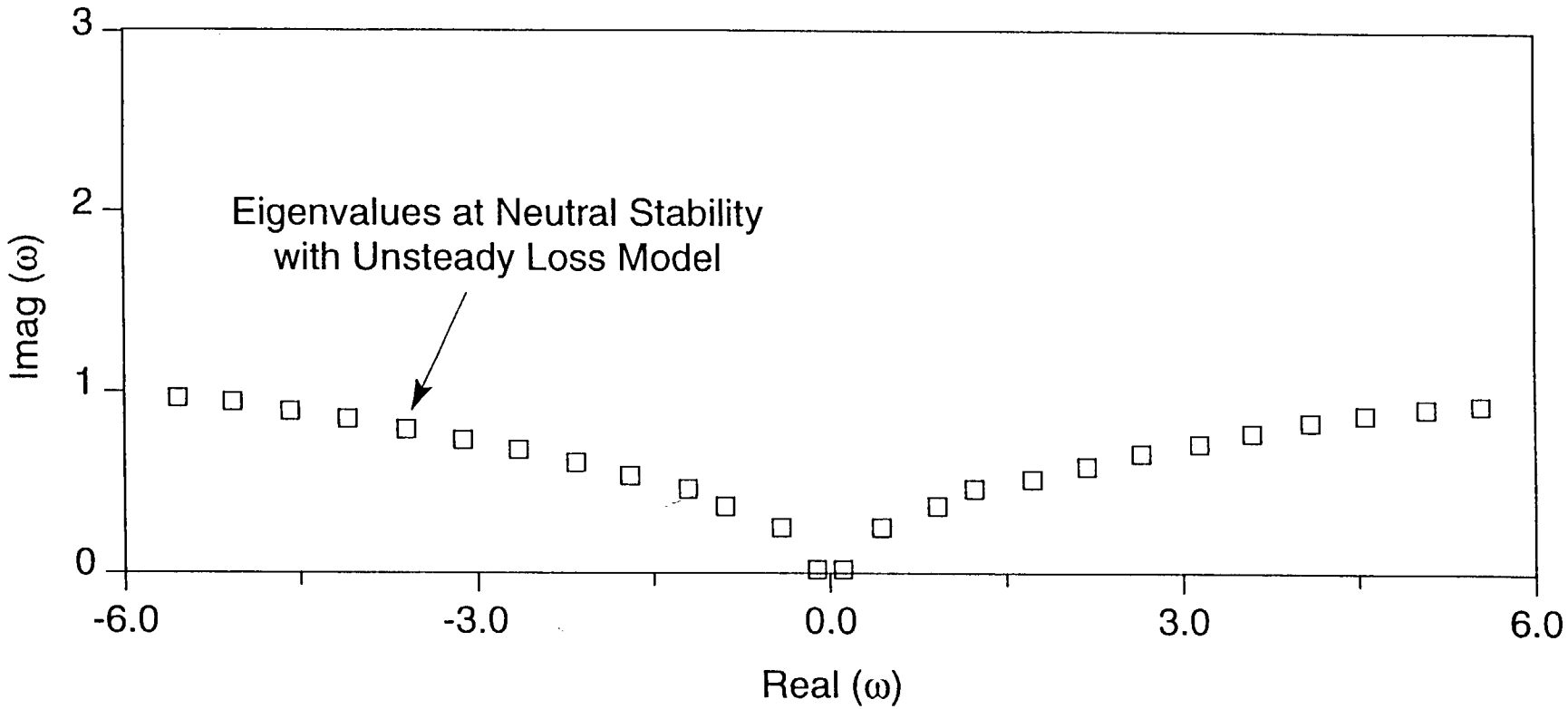

Fig. 10: Distribution of eigenvalues at neutral stability – unsteady loss model vs. quasi-steady analysis; results from quasi-steady model lie on Real (ω) axis.

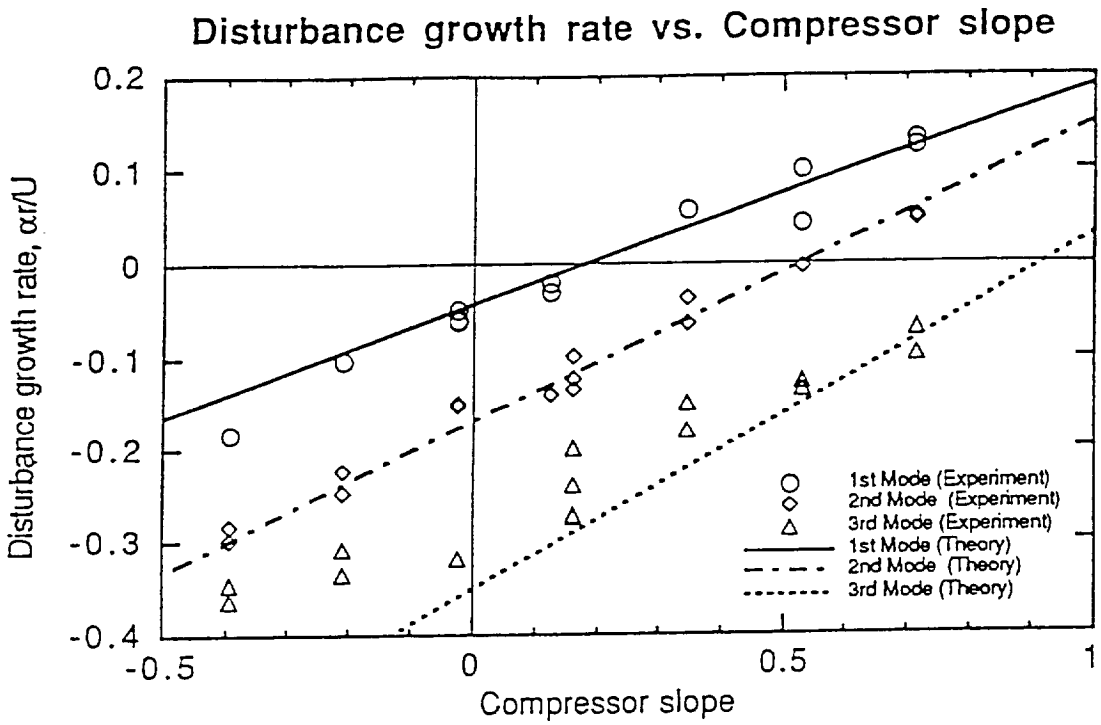

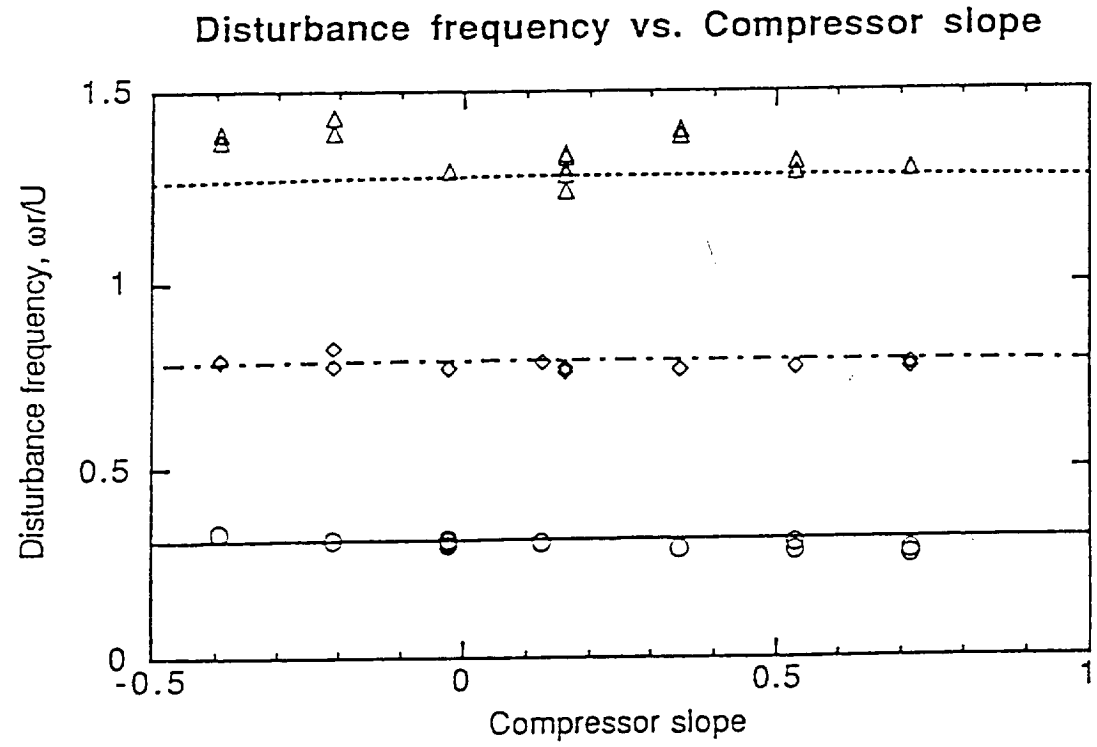

Fig. 11: Theory vs. experiment; three-stage compressor.

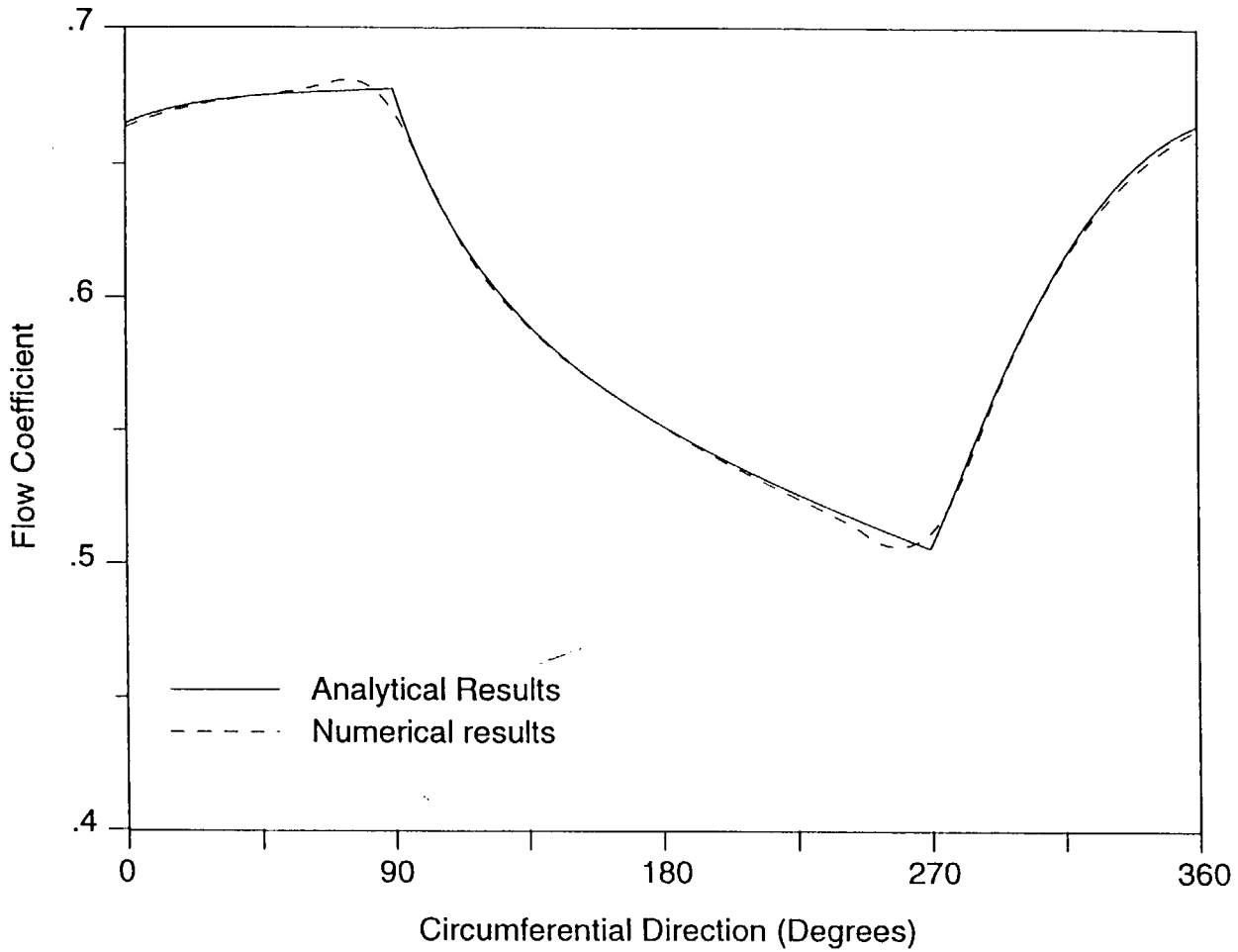

Fig. 12: 2-D case: assessment of ICFM against analytical results.

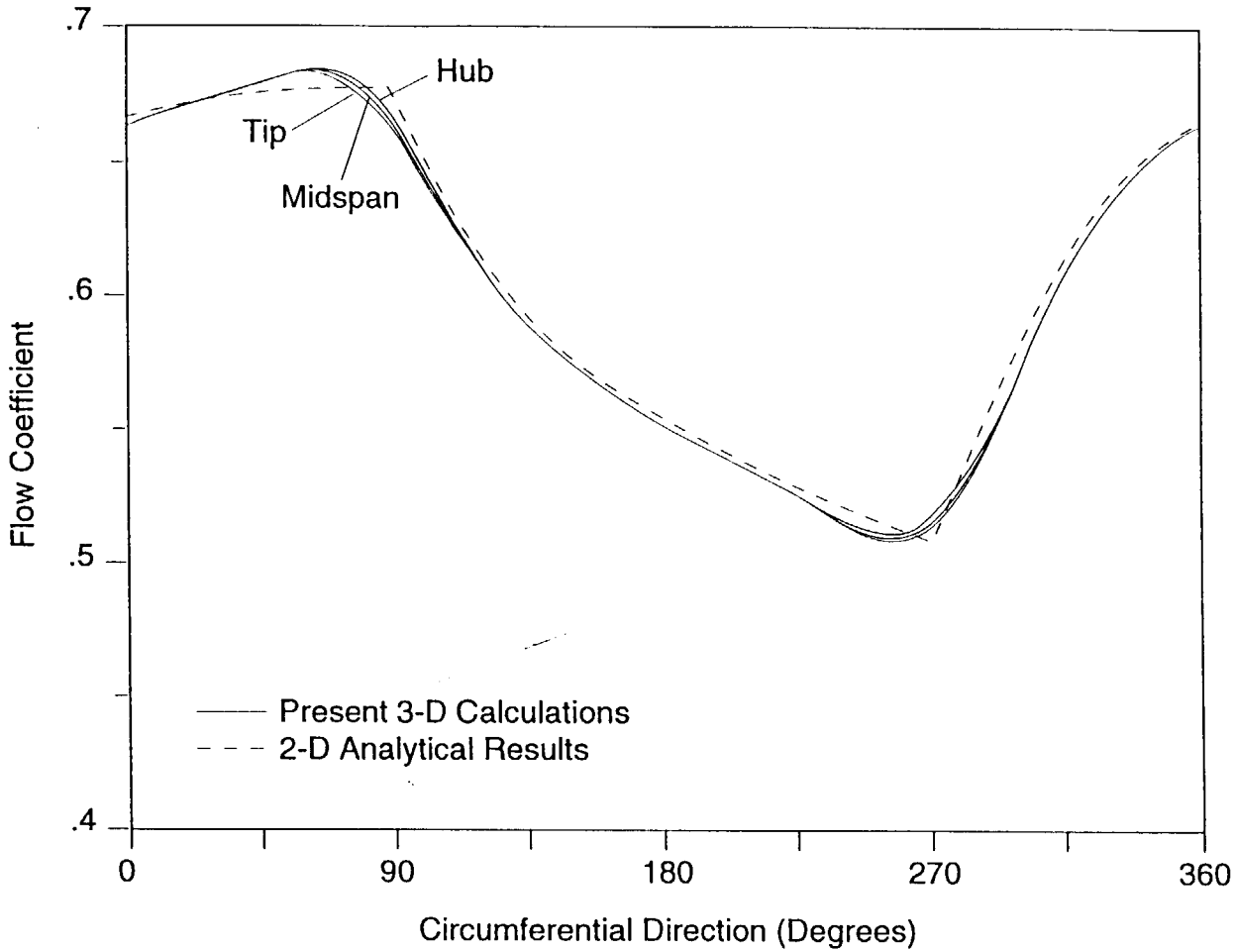

Fig. 13: 3-D results for high hub-to-tip ratio compressor based on ICFM compared with known 2-D analytical results.

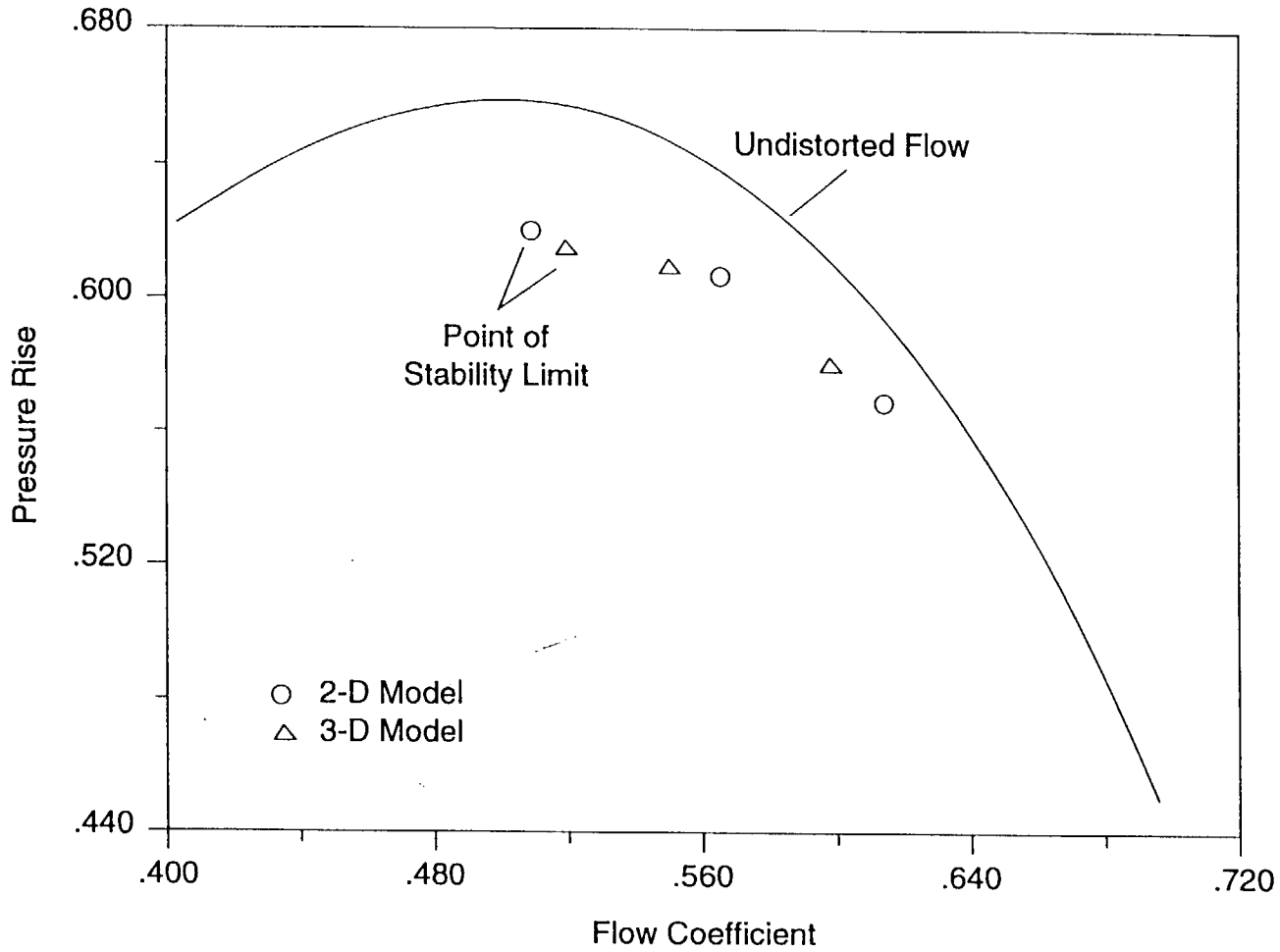

Fig. 14: Pressure rise characteristics of low hub-tip ratio compressor subjected to far upstream square wave distortion (i.e. a 2-D circumferential distortion).

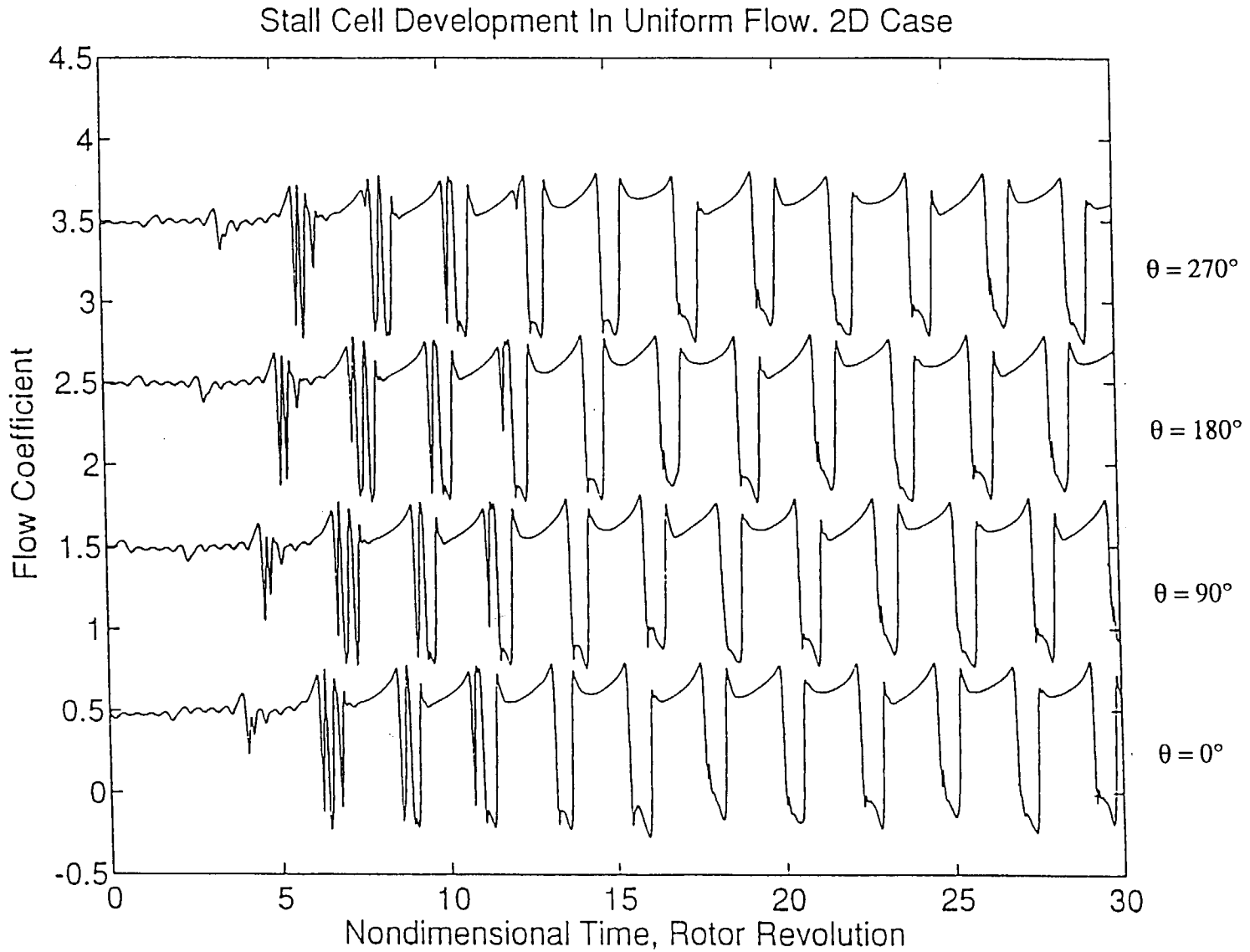

Fig. 15a: ICFM computed temporal and spatial evolution of stall cell in two-dimensional uniform flow situation.

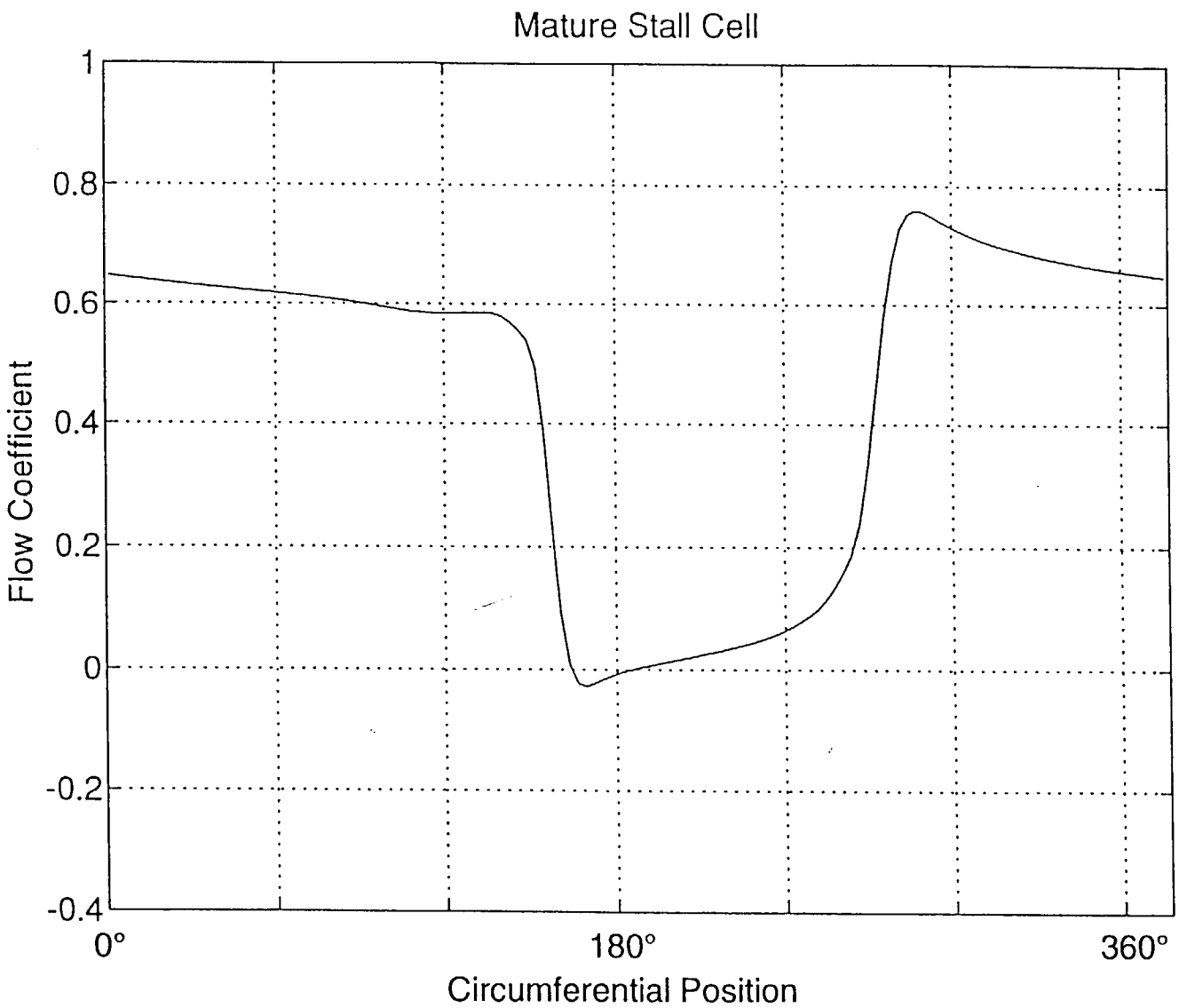

Fig. 15b: ICFM computed stall cell pattern.

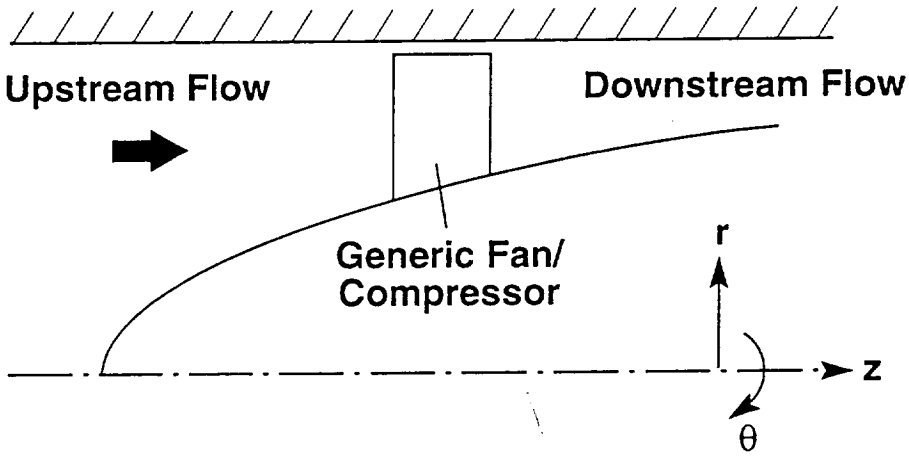

Fig. 16: Geometry of a representative compressor annulus.

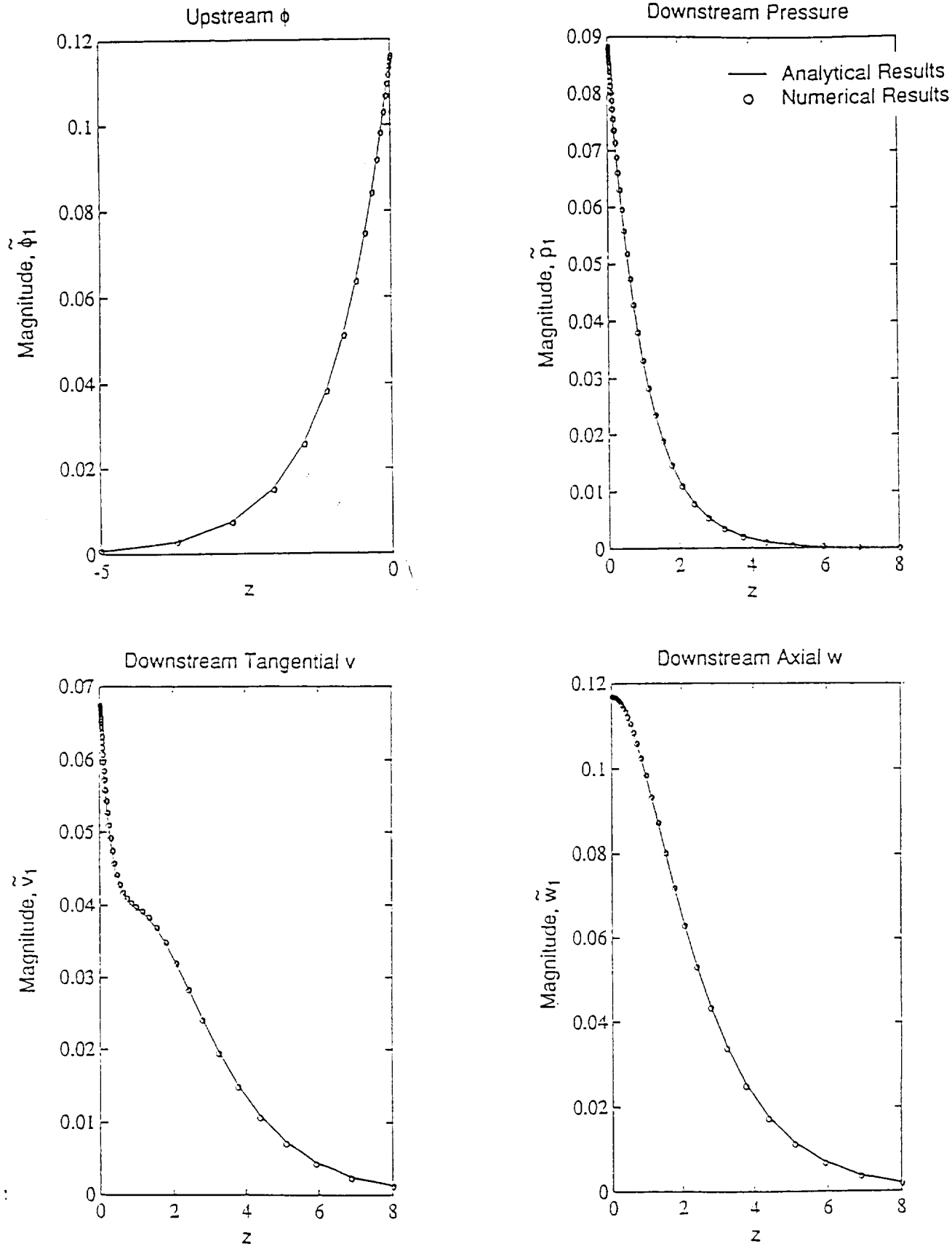

Fig. 17: Flow variables computed based on current stability calculation technique vs. analytical solution for two-dimensional flow situation.

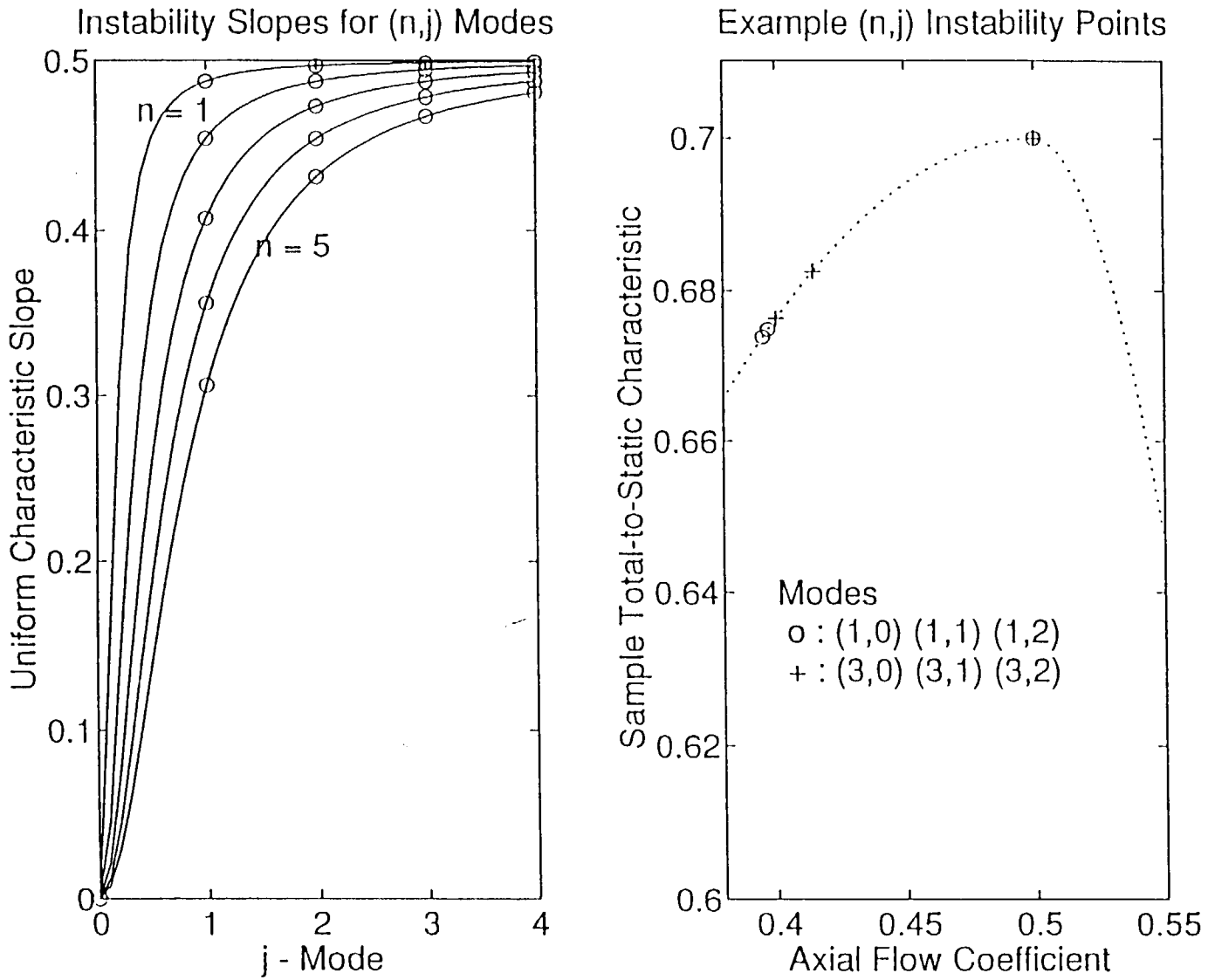

Fig. 18: Effect of radial dependence on instability onset.

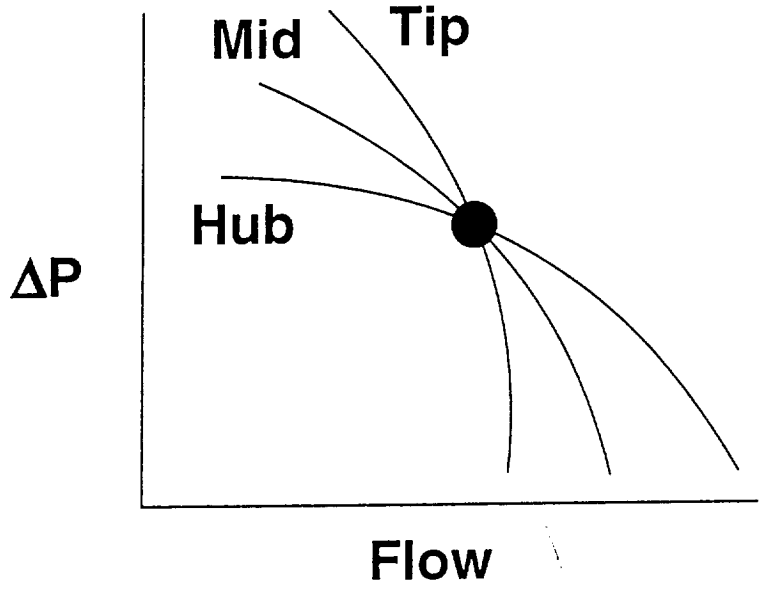

Fig. 19: Hub-to-tip variation of slope of stage pressure rise characteristics.

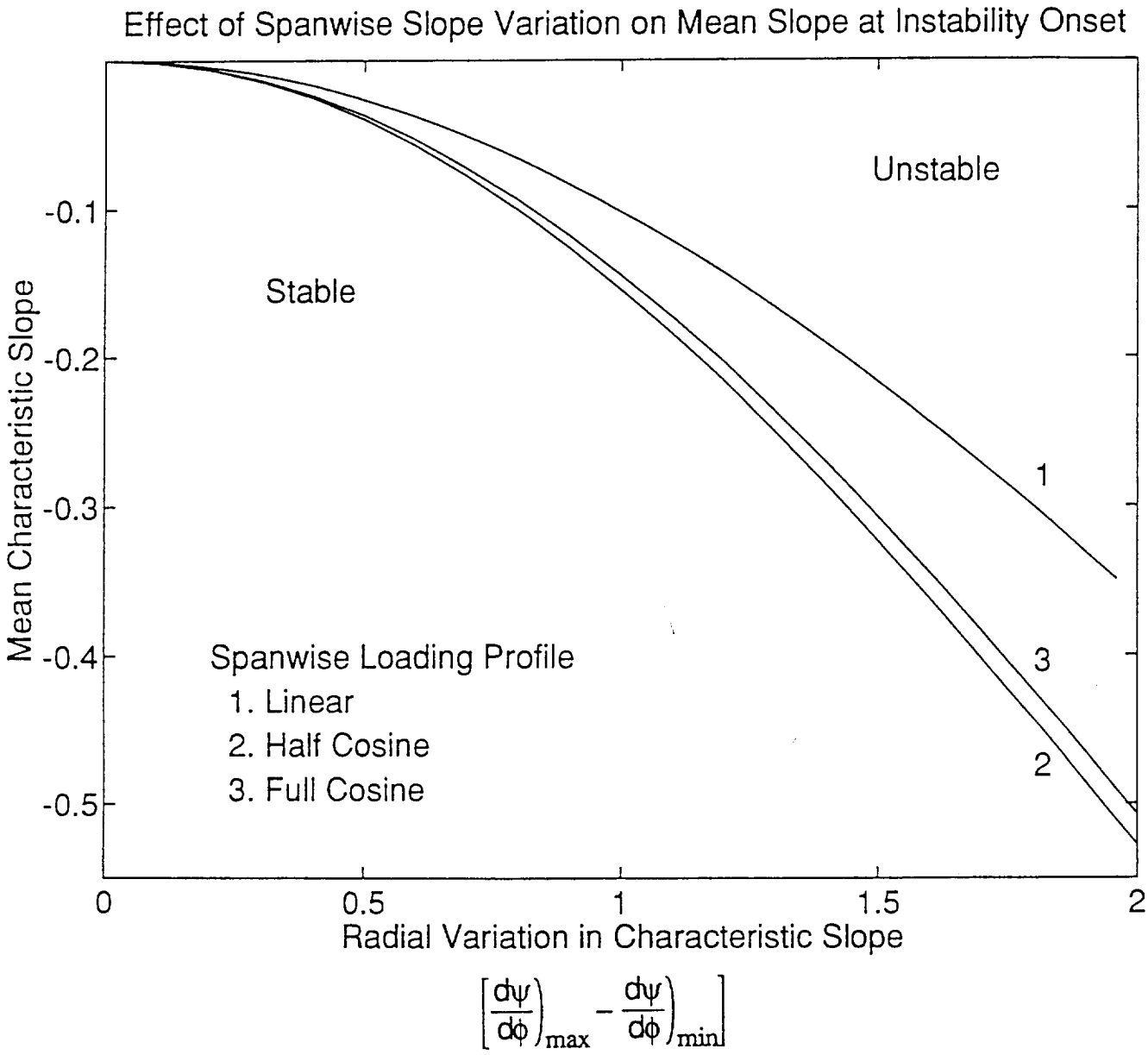

Fig. 20: Effect of hub-to-tip variation in stage pressure rise characteristics on instability onset.